

Electrochemical production of sustainable hydrocarbon fuels from CO₂ co-electrolysis in eutectic molten melts

Ossama Al-Juboori¹, Farooq Sher^{2,*}, Ushna Khalid³, Muhammad Bilal Khan Niazi⁴, George Z. Chen^{1,5*}

¹*Department of Chemical and Environmental Engineering, University of Nottingham, University Park, Nottingham NG7 2RD, UK*

²*School of Mechanical, Aerospace and Automotive Engineering, Faculty of Engineering, Environment and Computing, Coventry University, Coventry CV1 5FB, UK*

³*Department of Chemistry, University of Agriculture, Faisalabad 38000, Pakistan*

⁴*School of Chemical and Materials Engineering, National University of Sciences and Technology, Islamabad 44000, Pakistan*

⁵*Department of Chemical and Environmental Engineering, Faculty of Science and Engineering, University of Nottingham Ningbo China, University Park, Ningbo 315100, China*

*Corresponding authors:

E-mail address: Farooq.Sher@coventry.ac.uk (F.Sher), George.Chen@nottingham.ac.uk (G.Chen)

Abstract

Due to the heavy reliance of people on the limited fossil fuel as energy resources, global warming has increased to severe levels due to huge CO₂ emission into the atmosphere. To mitigate this situation, a green method is presented here for the conversion of CO₂/H₂O into sustainable hydrocarbon fuels via electrolysis in eutectic molten salts ((KCl-LiCl; 41:59 mol%), (LiOH-NaOH; 27:73 mol%), (KOH-NaOH; 50:50 mol%), (Li₂CO₃-Na₂CO₃-K₂CO₃; 43.5:31.5:25 mol%)) at the conditions of 1.5–2 V and 225–475 °C depending upon molten electrolyte used. Gas chromatography (GC) and GC-MS techniques were employed to analyse the content of gaseous products. The electrolysis results in hydrocarbon production with maximum 59.30, 87.70 and 99% faraday efficiency in case of molten chloride, molten hydroxide and molten carbonate electrolytes under the temperature of 375, 275 and 425 °C

31 respectively. The Gas chromatography (GC) with FID and TCD detectors and GC-MS analysis
32 confirmed that the H₂ and CH₄ were the main products in case of molten chlorides and
33 hydroxides at 2 V applied voltage while longer hydrocarbons (>C₁) were obtained only in
34 molten carbonates at 1.5 V. Through this manner, electricity is transformed into chemical
35 energy. The heating values obtained from the produced hydrocarbon fuels are satisfactory for
36 further application. The practice of molten salts could be a promising and encouraging
37 technology for further fundamental investigation for sustainable hydrocarbon fuel formation
38 with more product concentrations due to its fast-electrolytic conversion rate without the use of
39 catalyst.

40

41 **Keywords:** Sustainable fuels; Molten salts; Co-electrolysis; Hydrocarbon fuels, Electrolyte
42 mixture; CH₄ and H₂ production.

43

44 **Introduction**

45 Over the past few decades, two major issues have captured the attention of scientists and
46 policymakers: global warming due to the increasing levels of carbon dioxide gas (CO₂) in the
47 atmosphere, and the rapid depletion of fossil fuels as an energy resource. To tackle these
48 complications, two solutions were proposed ^{1, 2}. The first solution is the use of renewable
49 energy resources such as wind, solar, nuclear or geothermal energy to minimize the greenhouse
50 gases' emission. While the second solution is the consumption of CO₂ to remove its excessive
51 concentration from the atmosphere and to enhance energy resources by converting it into
52 hydrocarbon fuels ^{3, 4}. Renewable energy resources do not involve CO₂ sequestration ⁵. So to
53 tackle CO₂ emissions ⁶, it was considered preferable to introduce some of the renewable energy
54 resources into an existing energy infrastructure as a “drop-in” form of energy. Examples of this
55 can include the synthesis of fuels or fertilizers from CO₂ or biomass ^{7, 8}.

56

57 At present, technologies studied for transforming CO₂ include chemical, photochemical,
58 electrochemical ⁹ and biological transformation into hydrocarbons ¹⁰, nano-carbons ¹¹,
59 nanotubes, and alcohols (methanol and ethanol) ⁴. However, these low-value hydrocarbons and
60 methanol produced at low system efficiencies undermine the rationale of this approach. The
61 process of CO₂ and water co-electrolysis at low temperatures (<100 °C) in aqueous media to
62 convert CO₂ to CO or hydrocarbon species was employed by scientists ^{12, 13}. However, a
63 suitable catalyst is necessary for this conversion process in order to reduce energy
64 consumption, improve reaction kinetics and product selectivity ^{14, 15}. Which results in low
65 hydrocarbon gas production due to the poor solubility of CO₂ in aqueous media and the
66 proximity of the electro-reduction potential of both water and CO₂. Consequently, limiting the
67 future use of this process.

68

69 Using high temperature electrolysis between 800 and 1000 °C, provided both thermodynamic
70 and kinetic advantages throughout the reduction of both CO₂ and H₂O. One thing to mention
71 here is that this process not only converts CO₂ into hydrocarbons but also able to produce
72 hydrogen fuel by the splitting of water. Hydrogen gas has been produced by various methods
73 such as plasma arc decomposition, bio-photolysis, coal gasification, dark fermentation,
74 artificial photosynthesis, electrolysis etc ¹⁶. But the electrolysis has proved successful among
75 all due to the good energy efficiency and low cost ¹⁷. Two types of cells were used for high
76 temperature electrolysis: those with solid oxide electrolytes and with molten salts ^{18, 19}.

77

78 Recently the use of solid oxide electrolysis cells (SOEC) has gained much interest in the
79 preparation of syngas (CO+H₂), hydrogen or methane gas from the CO₂-H₂O co-electrolysis
80 ^{20, 21}. However, certain limitations such as low production rate, specific electrode materials,

81 higher production costs, lower durability and high energy utilization, became the reason for
82 their rejection on industrial scale implementation ²². Molten salts exhibit the same chemistry
83 regarding CO₂ and H₂O reduction as in SOEC except that CO₂ can be also reduced to carbon
84 ²³ in addition to carbon monoxide depending on the operating conditions. Which can thereby
85 affect the products. Deposited carbon on cathode can facilitate the formation of different kinds
86 of hydrocarbons (rather than CO) in case of molten salt electrolysis. Because as soon as the
87 fresh carbon deposit on cathode it reacts immediately with hydrogen gas produced via water
88 reduction on the metal cathode surface itself, resulting in the formation of hydrocarbons ²⁴.

89

90 Molten salts are preferred over solid oxides regarding CO₂-H₂O co-electrolysis for a variety of
91 reasons. Besides a wide electrochemical window, high electric conductivity, relatively low
92 cost, reactivity with CO₂ and no need of specific electrode materials (Ni-YSZ, La_{1-x}
93 Sr_xMnO₃/YSZ) make them suitable candidates for this process. Moreover, the possibility of
94 carbon or CO hydrogenation after electrolysis in molten salts is much more significant ^{25, 26}.

95 Molten salts with some limitations such as slight corrosion activity particularly at high
96 temperature and relatively high energy utilisation to maintain the heat for molten salt to avoid
97 the solidification ²⁷, can still be employed to produce hydrocarbon gas or liquid fuels ^{28, 29}.

98 Recently carbon nanotubes (CN) and carbon nano-fibrils (CNF) have been produced by using
99 molten chlorides ³⁰, molten carbonates ³¹ and molten hydroxides with sufficient conditions of
100 electrolyte combinations, electrode materials, current and temperature etc ³²⁻³⁴.

101

102 Moreover, recent investigations also showed the production of syngas (CO, H₂) and methane
103 by employing molten carbonates (Li₂CO₃-Na₂CO₃-K₂CO₃) ^{24, 35}. There is lack of literature of
104 finding suitable molten salt electrolyte for the co-electrolysis of CO₂ and H₂O to produce
105 hydrocarbon fuels (CH₄ or longer chain). To the best of our knowledge, molten hydroxides

106 ((LiOH-NaOH; 27:73 mol%), (KOH-NaOH; 50:50 mol %)) and molten chlorides (LiCl-KCl;
107 58.5:41.5 mol%) have never been evaluated for CO₂ to methane conversion. And molten
108 carbonates (Li₂CO₃-Na₂CO₃-K₂CO₃; 43.5:31.5:25 mol%) have never been studied particularly
109 for higher hydrocarbon fuel (>C₁) production via CO₂-H₂O co-electrolysis. So this study aims
110 to fill the research gap in the literature.

111
112 This study systematically investigates the hydrocarbon fuel production by employing CO₂-H₂O
113 co-electrolysis by using different types of molten electrolytes: molten chloride (LiCl-KCl;
114 58.5:41.5 mol%), molten hydroxide ((LiOH-NaOH; 27:73 mol%), (KOH-NaOH; 50:50
115 mol%)) and molten carbonate (Li₂CO₃-Na₂CO₃-K₂CO₃; 43.5:31.5:25 mol%) at variable
116 conditions of temperature and voltage depending upon the molten salt. Two feed gas insertion
117 methods are also employed; gas flowing over the electrolyte surface (GFOE) and gas flowing
118 inside the electrolyte (GFIE). The effect of different variables including; faradays efficiency,
119 energy consumption and heating values at variable conditions of temperature and voltage are
120 studied. Moreover, the product formation by electrolysis is confirmed by GC (using FID and
121 TCD detectors) and GC-MS.

122 **Experimental**

123 **Chemicals**

124 Lithium carbonate (Li₂CO₃; ≥99%), sodium carbonate (Na₂CO₃; ≥99.5%), potassium
125 carbonate (K₂CO₃; ≥99%), lithium chloride (LiCl; 99%), potassium chloride (KCl; >99.9%),
126 lithium hydroxide (LiOH; ≥98% powder), sodium hydroxide (NaOH; ≥98% pellets), and
127 potassium hydroxide (KOH; 90% flakes) were purchased from Sigma-Aldrich, USA. Carbon
128 dioxide (CO₂; 99.99%) and argon (Ar; 99.99%) were procured from Air products. Labovac 10
129 mineral oil was got from Jencons.

130 **Electrochemical performance measurement**

131 The electrochemical processes were performed by using four combinations of molten salts as
132 electrolytes. The key point of choosing these combinations of molten salts is due to their low
133 melting points and the ability to work at operating temperatures, as low as possible, keeping
134 them in liquid state to enable electrolysis and promote hydrocarbon formation. The
135 composition selection of binary mixtures (LiCl-KCl, LiOH-NaOH and KOH-NaOH) was done
136 on the basis of thermodynamic phase diagrams as illustrated from the **Fig. S1**. The ternary
137 phase diagram (**Fig. S2**) is clearly indicating the composition selection of ternary molten salt
138 mixture (Li₂CO₃-Na₂CO₃-K₂CO₃). Therefore, the salts selected for this study along with their
139 compositions are: LiCl-KCl (58.5: 41.5 mol%), LiOH-NaOH (27: 73 mol%), KOH-NaOH (50:
140 50 mol%) and Li₂CO₃-Na₂CO₃-K₂CO₃ (43.5: 31.5: 25 mol%), having eutectic melting
141 temperatures of 361, 218, 170 and 397 °C respectively. The electrolyte salts were dried in an
142 oven at 200 °C for 4 h at atmospheric pressure before their mixing to remove any sort of water
143 impurity.

144
145 Then electrolytes were poured into a crucible present inside a corrosion resistant electrolyser's
146 retort. Which was built in house with a flange type cover using the 316-grade stainless steel to
147 shape the reactor to provide and control the environment needed for the molten salt electrolysis.
148 The dimensions of the retort were 130 mm internal diameter, 7.5 mm wall thickness and 800
149 mm vertical length. On the flange cover, there were some holes drilled for the insertion of
150 ceramic tubes (for anode and cathode gas collection), observation purposes and sealing. The
151 retort was inserted centrally in the furnace. In the retort, a stainless-steel stand was placed and
152 a refractory brick mounted on it and above its alumina crucible containing pre-melted molten
153 salt electrolyte (about 100 g) was placed. The two-electrode mode experimental set-up used
154 here is a continuous system with small scale for electrolysis and hydrocarbon production. The

155 electrolysis is conducted by using titanium metal (Purity: 99.99%, Good fellow Cambridge
156 Ltd) as cathode and graphite (Purity: 99.99%, Advent Research Materials) as anode^{36,37}.

157

158 A small rate of gas (CO₂; 48.4%, + H₂O; 3.2% + Ar; 48.4%) flows continuously inside the
159 reactor where hydrocarbons and O₂ gases are produced inside the molten salts on the cathode
160 and anode surfaces respectively during the electrolysis. And the products are collected at
161 different time intervals. This process is done by employing the Agilent E3633A 20A/10V
162 Auto-Ranging DC Power Supply and a laptop with an EXCEL add-in to collect the
163 instrumentation data. Two electrode tube gas outlets were present, each connected to another
164 Dreschel bottle containing the mineral oil to observe the outlet gases produced and reduce
165 electrolyte contamination. Gas product samples were collected using a tedler 1 L (SKC Ltd.)
166 gas bag via a connection from the cathodic gas tube. The electrolyser setup is a modified form
167 of previously used setups³⁸. The schematic representation of experimental setup is shown in

168 **Fig. 1**

169

170 To avoid their mixing, the argon gas was used which pushed the gaseous products into their
171 respective bags. Moreover, the study is carried out with two modes of feed gas insertion inside
172 the reactor for each electrolyte; gas flowing over the electrolyte surface (GFOE) and gas
173 flowing inside the electrolyte (GFIE) for the comparison of hydrocarbon production in both
174 cases. The first method (GFOE) has been used to minimize the chances of solid material's
175 production (carbon, carbon nanotubes, graphene, carbonates solidification)^{34,39} and to produce
176 gaseous hydrocarbon products preferably. The current efficiency was calculated from the **Eqs.**

177 **(1-2):**

$$\text{Current efficiency} = \frac{Q_x}{Q_T} \times 100 \quad (1)$$

$$Q_x = nNF \quad (2)$$

178 where Q_x is the charge required for the amount of individual product produced, n is the number
179 of electrons required, F is the charge of one electron which equals 96485 col and Q_T is the total
180 charge calculated from the area under the current vs time curve.

181 **Characterization**

182 Gas chromatography (GC) (PerkinElmer Clarus 580) was used to analyse the gas products
183 generated from electrolysis with detectors such as the flame ionization detector (FID) and
184 thermal conductivity detector (TCD) for organic compound analysis and a wide range of both
185 organic and inorganic species respectively. The gaseous product species in the sample were
186 identified and quantified by comparison with two different calibration gas standards. The first
187 one is the permanent gas standard with composition of H₂ 10%, CO₂ 10% and CO 40% for
188 TCD detector and the second standard calibration gas contains ethene (C₂H₄) 0.2%, propylene
189 (C₃H₆) 0.2%, 1-butene (C₄H₈) 0.2%, 1-pentene (C₅H₁₀) 0.2%, methane (CH₄) 20%, ethane
190 (C₂H₆) 10%, propane (C₃H₈) 5%, n-butane (C₄H₁₀) 2%, n-pentane (C₅H₁₂) 1% for the FID
191 detector.

192

193 The remaining composition of both gas standards was balanced with helium gas. The GC
194 graphs for different calibration gas standards are shown in **Fig. 2** for the comparison of
195 electrolysis gaseous products. Furthermore, the samples were analysed by a different
196 sophisticated GC instrument (Agilent 7890B) attached with a mass spectrometer (JEOL
197 AccuTOF GCX) for longer chain hydrocarbons detection. Gas detecting tubes from GASTEC
198 (ai-cbss Ltd.) were used to analyse the feed gas compositions for CO₂ and H₂O contents. The
199 feed gas composition with CO₂ (48.4%) + H₂O (3.2%) + Ar (48.4%) was kept same for all the
200 experiments. GASTEC 2HH is characterised to detect the higher contents of CO₂ from 5 to
201 40% of the feed gas, with the change in colour from orange to yellow.

202

203 The GASTEC30 tube can analyse water content in the range of 0–18 mg/L, and it contains
204 $\text{Mg}(\text{ClO}_4)_2$. However, the colour here will change from yellowish green to purple. After the
205 analysis of cathodic gas sample, the concentration of each gas compound (M_{gas}) was calculated
206 as followed by the **Eq. (3)**:

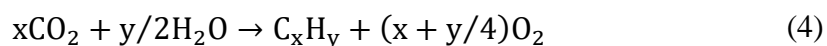
$$M_{\text{gas}} = \frac{A_{\text{gas}}/\bar{F}_i}{A_s/M_s} \quad (3)$$

207 where M_{gas} is the concentration (%) of individual gas in the sample. M_s is the concentration
208 (%) of the specific standard gas in the sample. A_{gas} is the area under the peak resulting from the
209 FID analysis for the individual gas ($\text{C}_2\text{-C}_5$) in the sample. A_s is the area under the peak resulting
210 from the analysis of the specific gas standard (CH_4). \bar{F}_i is the response factor for each gas.

211 **Results and discussion**

212 **Optimization of electrolytes**

213 The selection of the molten salt is done based on the ability to generate hydrocarbon fuels from
214 the co-reduction of CO_2 and H_2O (**Eq. (4)**). The combination of a hydrocarbon molecule starts
215 ideally from the two known element sources: carbon (C) and hydrogen (H). Both of these
216 elements can be effectively formed from electrochemical conversion via an appropriate molten
217 salt.



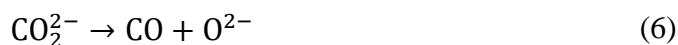
218

219 Generally, the presence of moisture with CO_2 gas in molten salt experiments is the basis for
220 generating H_2 and CH_4 during electrolysis in most cases and provide feasibility to the reactions

221 ^{40, 41}.

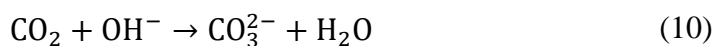
222 Molten chloride electrolyte

223 The attractive characteristic in the molten chloride case is the probability of producing CO or
224 C directly from CO₂ reduction in the presence or absence of a carbonate ion⁴¹. Carbonate ions
225 (if added externally) are used as an important additive to molten chlorides to provide the oxide
226 ions required for performing CO₂ reduction^{42, 43}. For absorbing more CO₂ gas into the molten
227 salt leading to increase in product yield from electrolysis, the addition of oxides or carbonate
228 salts into the molten chloride is considered preferable. But one drawback exhibited by this
229 process was the increase in applied voltage and working temperature of resulting molten salt
230 mixture. Which is not the favourable condition for hydrocarbon production⁴⁴. So to tackle this
231 problem, molten chloride electrolyte is used in this study for hydrocarbon production without
232 any externally added oxide or carbonate salts. In the absence of H₂O and carbonate ions, the
233 reduction of CO₂ to carbon or CO can be done in several steps as seen from the **Eqs. (5-7)**⁴⁵.

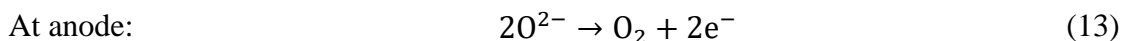
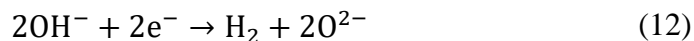
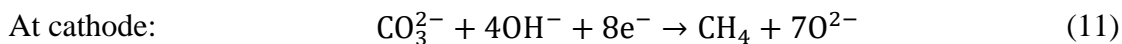


234
235 In the presence of steam beside CO₂ in the feed gas, the reduction of CO₂ becomes more
236 feasible as CO₂ can react with hydroxide ions released from the primary reduction of H₂O
237 through to the one-electron transfer reaction. Moreover, carbonate ions can be generated even
238 from molten chloride through the reaction of CO₂ with oxide ions emitted in turn after the
239 direct reduction of H₂O to H₂ gas (**Eq. (9)**)⁴⁶. The carbonate ions can then be electro-reduced
240 in turn to carbon or CO and produce hydrocarbon by reacting with H₂. The overall reaction
241 occurring at electrodes can be summarised from the **Eqs. (11-13)**.





242 Overall reaction



243

244 It is preferable to perform CO₂-H₂O co-electrolysis at temperatures even lower than the 400 °C
245 to form the hydrocarbons feasibly. For that purpose, electrolysis was performed at 375 °C and
246 2V using molten chloride (LiCl-KCl; 41: 59 mol%) with two modes of gas insertion: GFOE
247 and GFIE. The feed gas in GFOE mode containing H₂O, CO₂ and Ar, was kept flowing over
248 the LiCl-KCl (41: 59 mol%) at 1.3 bar. The feed gas pressure was applied slightly over 1 atm
249 to increase CO₂ activity and thus the opportunity of improving reduction inside the molten
250 chloride.

251

252 The same experiment was performed at the above conditions using a feed gas containing H₂O
253 with no CO₂. Both experiments in GFOE mode are performed to see the solubility of CO₂ and
254 thus its activity inside molten chlorides. Carrying out electrolysis at 2 V and 375 °C, it can be
255 seen from **Fig. 3** that there is a small difference between the two current curves resulting from
256 electrolysis in both cases. However, the current was still relatively high in both cases and
257 gradually decreased with time. The decline in current can be imputed generally to the drop of
258 oxidant concentration (H₂O, CO₂) that is reduced on the cathode surface due to the
259 accumulation of new products (such as H or H₂ bubbles) as there is no renewal action on the
260 cathode surface during electrolysis. Also, it can be noted that the current was slightly higher in
261 the case where CO₂ gas was absent basically due to the obstruction of CO₂ gas against H₂O

262 reduction on the electrode, particularly at high pressures through the possible reduction of CO₂
263 to CO₂²⁻ (**Eq. (5)**).

264

265 Despite some spikes noticed in the red curve in **Fig. 3**, it can be seen that the drop of the curves
266 in both cases was quite the same confirming the weak effect of CO₂ inside the molten chloride
267 in GFOE mode. So due to CO₂ weak effect, the hydrocarbon could not be produced in this case
268 (GFOE mode). The GFIE mode of gas feed introduction was chosen as an appropriate way to
269 increase CO₂ concentration and solubility (and reactivity) inside the molten chloride and collect
270 the maximum rates of hydrocarbon products at atmospheric pressure. The rates of H₂ and CH₄
271 production, collected from the cathodic tube, changed significantly after the first 30 and 60 min
272 of electrolysis due to the process of carbonate ions formation as can be seen by the comparison
273 of **Fig. 4(a)** and **(b)**. Where the higher production rates of CH₄ (0.67 μmol/h cm²) and H₂ (32.00
274 μmol/h cm²) with higher faraday efficiency (59.30%) were found after the first 30 min of
275 electrolysis (**Fig. 4(a)**). While the lower production rates of CH₄ (0.39 μmol/h cm²) and H₂
276 (19.10 μmol/h cm²) with faraday efficiency (30.50%) were obtained after 60 min of electrolysis
277 (**Fig. 4(b)**) in molten chloride (LiCl-KCl; 41: 59 mol%).

278

279 The lower faraday efficiency (30.50%) was attributed due to the higher CO₃²⁻ ion formation
280 leading to the subsequent conversion to C or CO with more energy consumption. The formation
281 of a carbonate ion can be justified due to the reaction of CO₂ with OH⁻ generated in the molten
282 chloride after the persistent reduction of H₂O as stated previously in **Eq. (10)**⁴⁶. It is interesting
283 to note that there is a clear increasing trend of CH₄ production in both **Fig. 4(a)** and **(b)** at a
284 lower current density of 20 mA/cm², which starts dropping off beyond this limit. The increase
285 in current density affects the products content. With the current density increase, the CH₄
286 production reached to an optimal value. After that further rise in current density results in

287 adverse effects on CH₄ production, greatly exceeding the minimum energy requirement of H₂
288 production that keeps CH₄ production at a lower level^{24,35}. Deng *et al.*³¹ stated that LiCl-KCl
289 electrolyte containing Li₂CO₃/CaCO₃ showed highest current efficiency of 80–85% at the
290 current density of 25 mA/cm², which dropped off by increasing current density for the
291 conversion of CO₂ to carbon.

292

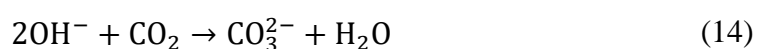
293 Comparing results for the two occasions as two gas samples were taken after 30 and 60 min, it
294 can be noted that the production rates of both gases (CH₄ and H₂) were higher in the first sample
295 after first 30 min of electrolysis as the electro-reduction of the carbonate ions (to carbon for
296 instance) had not commenced yet. Thus, the reduction of H₂O to H₂ was not significantly
297 affected. The reaction of CO₂ with OH⁻ can be confirmed in the molten chloride for the second
298 sample as the concentration of CO₂ reduced from 34.80 to 4.80% (**Table 1**). The hydrocarbon
299 production confirmed through GC analysis (with FID and TCD detectors) is shown in **Fig. 5**
300 where the FID signals are showing the production of methane with the peak at 2.11 retention
301 time while TCD signals are clearly representing the peaks of H₂, O₂ and CO₂. No CO can be
302 detected in the molten chloride in both cases.

303

304 Thus, the best product concentrations are obtained in case of LiCl-KCl (41: 59 mol%)
305 electrolyte from GFIE mode at the first 30 min of electrolysis rather than prolonged electrolysis
306 (60 min). This is because of the formation of carbonate ions in case of prolonged electrolysis,
307 which are reduced to the C or CO gases with the consumption of more energy (**Table 1**). Ijije
308 *et al.*⁴⁷ reported the CO₂ conversion into carbon films or CO in LiCl-KCl-CaCl₂-CaCO₃ molten
309 salt at 520 °C. Similarly, the absorption and conversion of CO₂ was also employed in molten
310 chloride electrolytes (CaCl₂-CaO and LiCl-Li₂O) at 900 and 650 °C respectively⁴⁸. Jianbang
311 *et al.*³⁰ has converted CO₂ by electrolysis in LiCl molten salt at 650 °C.

312 Molten hydroxide electrolyte

313 The molten hydroxide salt is preferred in the case of hydrogen production leading to
314 hydrocarbons formation. Hydrocarbon molecules can be formed basically through a H₂
315 reaction with either C or CO as the same mechanism for molten chlorides ⁴⁹. In most
316 experiments using molten hydroxides, the conversion of CO₂ was very high but the
317 hydrocarbon yields were still low. This can be attributed generally to the reaction of CO₂ with
318 hydroxide ions ⁵⁰.



319
320 Therefore, CO₂ must be diluted to lower concentrations by mixing with argon gas before
321 introduction to the electrolyte, as this action can help to reduce the reactivity of CO₂ with the
322 salt, driving reaction (**Eq. (14)**) to the left side. The formation of carbonate ions need to be
323 reduced to provide enough time for the prospect of electro-reduction during electrolysis.
324 However, CH₄ gas can be formed by another way in case of molten hydroxide electrolysis (**Eq.**
325 **(15)**) ⁵¹.



326
327 Thus, the abundance of hydrogen gas from rapid H₂O reduction in molten hydroxides can
328 contribute towards driving reaction (**Eq. (15)**) to CH₄ formation. The hydrocarbon production
329 in molten hydroxide (LiOH-NaOH: 27: 73 mol%) performed in two modes: GFOE and GFIE
330 at the conditions of 2 V applied voltage and 275 °C, is shown in **Fig. 6 (a)** and **(b)**. The results
331 indicate a distinct variation in the production rates due to the variation in gas feed modes. This
332 outcome can be attributed to the weak reduction of CO₂ in the salt in GFOE mode. The
333 hydrocarbon production rate was significantly improved when the feed gas insertion method
334 was changed from GFOE to GFIE. It can be seen from the **Fig. 6 (a)** to **(b)** that the CH₄ rate

335 increased largely from 1.02 to 6.12 $\mu\text{mol/h cm}^2$ by moving from GFOE to GFIE mode as CO_2
336 was promoted to dissolve in the salt.

337

338 Therefore, the prospect of direct reduction of CO_2 to CO_2^{2-} and CO can occur in the LiOH-
339 NaOH salt. At the same time, the H_2 rate decreased from 1142.80 $\mu\text{mol/h cm}^2$ to just 185.00
340 $\mu\text{mol/h cm}^2$, confirming the possible transformation of CO_2 or CO to hydrocarbons.
341 Nevertheless, high faraday efficiency (87.70%) in the GFOE mode rather than (15.00%) in the
342 GFIE mode was due to the higher H_2 production rate. On the other hand, low faraday
343 efficiencies in GFIE mode were obviously because of their lower production values from the
344 slow reduction of CO_2 to CO compared with rapid H_2 production. Moreover, the optimal
345 current density range found for hydrocarbon production in case of LiOH-NaOH salt was 80–
346 85 mA/cm^2 .

347

348 Hydrocarbon production inside the molten hydroxide can be confirmed actually by the
349 existence of CO fuel with the cathode gas product. CO can be formed from CO_2 reduction as
350 in molten chloride experiments. But the scarcity of CO gas found in the cathodic products in
351 both electrolytes can be interpreted due to (1) a lack of CO_2 direct reduction to CO but the
352 formation of CH_4 occurs by the reaction of CO_2 with excess H_2 and (2) the produced amount
353 of CO during electrolysis in all cases was too little as CO can rapidly react with excess H_2 to
354 produce CH_4 . The formation of gaseous product (CH_4) was confirmed from GC analysis with
355 FID detector while H_2 , O_2 and CO_2 were confirmed by TCD detectors for the GFIE mode (**Fig.**
356 **7**). And obtained values are presented in **Table 2**. The presence of very small peak of CO in
357 **Fig. 7 (b)** is providing the indication of higher methane production rates than molten chloride
358 case.

359

360 As the GFIE mode provided higher production values of methane in case of molten hydroxide
361 so the experiment was repeated using KOH-NaOH (50:50 mol%) due to its low working
362 temperature, under the conditions of 2V applied cell voltage and 225 °C with GFIE mode only.
363 Although the temperature used here was slightly lower than 275 °C as used for LiOH-NaOH
364 (27: 73 mol%) molten salt but the production rates of H₂ (164.70 μmol/h cm²) and CH₄ (6.12
365 μmol/h cm²) with faradaic efficiencies (17.90%) were almost same (**Fig. 6 (c)**). Moreover, the
366 composition and concentration (vol%) of other cathodic product gases were also same (**Table**
367 **2**). But one limiting factor was the lower resulting current in the case of KOH-NaOH (50:50
368 mol%) molten salt than LiOH-NaOH (27: 73 mol%) (**Fig. 8**). Moreover, the potentials for
369 carbon deposition or carbon monoxide evolution are more positive than the deposition
370 potentials of Li metal for the case of LiOH.

371
372 In contrast, in the case of KOH, the potential for the formation of C or CO is more negative
373 than the deposition potential of potassium. The comparison suggests that carbon/CO evolution
374 leading to the formation of methane is the more preferential product in the presence of LiOH
375 as also observed in the previous study⁴⁴. Therefore, the KOH-NaOH (50:50 mol%) electrolyte
376 use was not preferred for hydrocarbon production. Consequently, the fuel production (H₂, CH₄)
377 was achieved in all cases of molten hydroxide electrolytes with different product composition
378 and concentration (vol%) as can be seen from **Table 2** but the best results were provided by
379 the LiOH-NaOH (27: 73 mol%) molten salt with GFIE mode than the other cases.

380 **Molten carbonate electrolyte**

381 The third kind of electrolyte used for hydrocarbon production is a ternary molten carbonate
382 mixture (Li₂CO₃-Na₂CO₃-K₂CO₃; 43.5: 31.5: 25.0 mol%) that is used in this research due to its
383 relatively low melting point of 394 °C. The formation of hydrocarbons can occur directly or
384 indirectly in a molten carbonate through the reaction of C with H₂ or CO with H₂ respectively

385 which are produced primarily from the independent reductions of CO₂ and H₂O^{28, 52}.
386 Subsequently, experiments conducted on this salt at a range of 400–450 °C, can be perfect
387 conditions for efficient hydrocarbon formation. In the case of electrolysis applied at conditions
388 of 1.5 V cell voltage and 425 °C, the maximum CH₄ production rate was achieved. It can be
389 seen from **Fig. 9** that a significant amount of CH₄ (1.10 μmol/h cm²), H₂ (4.40 μmol/h cm²)
390 and CO (11.70 μmol/h cm²) were obtained at the lower current density range of 4–6 mA/cm².

391
392 The relevant faraday efficiency obtained was 56.20% for the production of CH₄, CO and H₂,
393 which were confirmed through GC analysis using FID and TCD detectors (see **Fig. 10**) with
394 production concentration values mention in **Table 3**. These production results are in agreement
395 with previous studies^{24, 25}. Wu et al.¹⁰ provided support to the conversion of CO₂ and H₂O to
396 methane in case of molten carbonate electrolysis. It is worth mentioning that H₂ and CO were
397 the predominant gases during the experiment. Moreover, the existence of CO as clearly noted
398 from **Fig. 9** and confirmed through GC analysis with TCD detector (see **Fig. 10 (b)**) in a
399 relatively significant amount (in comparison to CH₄), can be imputed to the individual
400 reduction of CO₂ to CO. Previous studies stated that CO itself cannot be expected in molten
401 carbonates at temperatures below 775 °C in cases where H₂O is absent⁴⁰.

402
403 However, some other authors have claimed that the formation of CO molecules can occur on
404 the cathode by CO₂ reduction at low temperatures (≤ 650 °C)⁵³. If the reduction of CO₂ to CO
405 is preferred, then H₂ gas will also be formed according to the water gas shift reaction (WGSR)
406 which occurs due to higher temperature (< 600 °C). In contrast, CO can be generated by the
407 reverse water gas shift reaction (RWGS)⁵⁰. However, WGSR is more feasible at temperatures
408 below 817 °C particularly in the event of high partial pressures of H₂O (up to 16.1 mmHg)
409 which is not the condition of present study case, so CO formation is preferred case than the H₂

410 production leading to the hydrocarbon production. The only GFIE mode is presented here due
411 to the same results obtained in both cases (GFOE and GFIE mode) because of the excessive
412 CO_3^{2-} ions already present in $\text{Li}_2\text{CO}_3\text{-Na}_2\text{CO}_3\text{-K}_2\text{CO}_3$ (43.5: 31.5: 25.0 mol%).

413
414 The existence of CO_2 gas in the cathodic gas products in all the molten electrolyte cases can be
415 due to the reasons as (1) some of the absorbed CO_2 from the molten carbonates can come out
416 with the cathodic product gas (2) CO_2 can be produced accompanying the various hydrocarbon
417 species (3) The difference between the inlet and outlet amounts of CO_2 cannot be ultimately
418 accounted as the transferred CO_2 to CO and hydrocarbon products. Some other amounts of CO_2
419 can be absorbed chemically in the molten salts (4) The 100 % CO_2 gas conversion cannot be
420 done. However, in large scale applications, the cathodic product gas with accompanied
421 amounts of CO_2 can be recycled repeatedly with feed gas to increase the ultimate CO_2
422 conversion rate. Ji *et al.*³⁵ was able to convert CO_2 and H_2O into CO, H_2 and CH_4 products at
423 600 °C with the current efficiency of 51% in Li-Na-K CO_3 -0.3LiOH electrolyte.

424 **Effect of temperature and voltage**

425 The optimum temperature used for the selected molten hydroxides was chosen on the basis of
426 the maximum CH_4 production obtained as can be seen from **Fig. 11**. The optimum temperatures
427 obtained were 375, 275, 225 and 425 °C for KCl-LiCl (58.5: 41.5 mol%), KOH-NaOH (50: 50
428 mol%), LiOH-NaOH (27: 73 mol%) and $\text{Li}_2\text{CO}_3\text{-Na}_2\text{CO}_3\text{-K}_2\text{CO}_3$ (43.5: 31.5 :25 mol%)
429 electrolytes respectively. The yields of hydrocarbon products (vol%) increased with the rise in
430 temperature up to an optimum temperature value while after that further rise in temperature
431 showed inverse effects in case of molten hydroxide and chloride salts. This was because the
432 CO_2 could not be transferred significantly to CO or hydrocarbon species because of the
433 prospects chemisorption of CO_2 in molten electrolytes at higher temperature. Ji *et al.*³⁵

434 provided the support to the obtained results by reporting that the reduction of co-electrolysis
435 of CO₂ and H₂O decreases by increasing the temperature.

436

437 While in the case of Li₂CO₃-Na₂CO₃-K₂CO₃, the highest CH₄ production increased up to 425
438 °C while after this temperature CH₄ production starts decreasing which might be due to the
439 increase in production values of other longer chain hydrocarbons (C₂-C₄) rather than CH₄ only.

440 This can be due to the increase in CO₂ gas solubility inside molten chloride at high temperature
441 (475 °C)⁵⁴. The cell voltage is a key variable that can affect energy consumption or current
442 efficiency but it can also improve the product properties at the same time^{49,54}. In case of molten
443 chlorides and hydroxides, the average current density increased drastically (20 to 70 mA/cm²)
444 and (70 to 120 mA/cm²) by increasing cell voltage from 2V to 3V as shown in **Fig. 12(a)** and
445 **(b)**. Likewise, CH₄ concentration (vol%) increased but with slower production rates.

446

447 However, the alkali metal electrodeposition starts occurring at a high cell voltage, consequently
448 affecting the current efficiencies of the products. So, at higher voltage, there is more waste of
449 energy due to the solid metal accumulation than the desired products⁵⁵. Therefore, the optimum
450 voltage selected for molten chlorides and hydroxides was 2V rather than 3V. To show the effect
451 of increasing cell voltage in molten carbonates, **Fig. 12(c)** illustrates the high difference
452 between the average current (4 to 25 mA/cm²) resulting from electrolysis applied at 1.5 and 2
453 V. The hydrocarbon formation was confirmed only at 1.5 V while carbon deposition occurred
454 due to the rise of voltage up to 2 V as also confirmed by previous studies^{54,56}. Performing both
455 runs at 425 °C, hydrocarbon formation at 2 V was rare and not noticeable. Consequently, the
456 optimum voltage selected for molten chloride and molten hydroxide was 2 V while 1.5 V for
457 molten carbonates.

458 **Formation of higher hydrocarbons**

459 The GC analysis performed using FID detector (**Fig. 10(a)**) showed that along with methane
460 production, various higher hydrocarbons were also detected in the case of molten carbonate
461 electrolyte. Which is further confirmed by GC-MS analysis (**Fig. 14**). The formation of
462 methane gas product can be justified due to the reaction of carbon or CO with H₂ as follows:

463



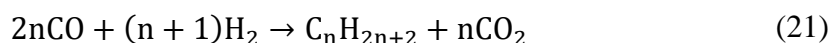
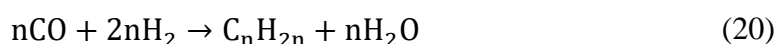
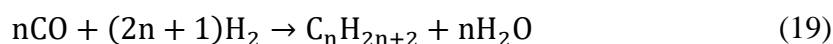
464

465 The Gibbs Energy values were determined at 425 °C (HSC Chemistry software, version 6.12;
466 Outokumpu Research) as this was the temperature of the experiment. It can be seen from the
467 first mechanism that the production of general hydrocarbons occurs basically from reaction in
468 **Eq. (16)** with the fresh deposit of carbon and adsorbed atomic hydrogen (H), produced in turn
469 from the individual reduction of CO₂ and H₂O respectively. On the other hand, the C₂, C₃ and
470 C₄ hydrocarbons, detected by GC analysis (with FID detector) are shown in **Fig. 13** along with
471 their production rate values (0.80, 0.50, 0.50 μmol/h.cm²) and faradays efficiency (total =
472 55.20%). It is important to note that the accumulative faraday efficiency for all products (C₁,
473 C₂, C₃, C₄, CO and H₂) obtained in case of molten carbonates electrolysis reached to the 95%
474 (**Table 3**).

475

476 The dominant peaks were of alkene products rather than alkanes in the GC analysis when
477 detected with FID detector, such as for ethene, propene, butene and pentene at 2.73, 3.06, 7.71
478 and 18.11 of retention times respectively. However, GC-MS analysis are also showing the
479 detection for some alkane products. The formation of alkene or alkanes can be justified due to

480 the (1) reaction of C or CO with hydrogen or (2) partial oxidation of methane in molten
 481 carbonate. Furthermore, in the first mechanism the CO produced in excess can react with H₂
 482 gas to produce higher hydrocarbons (C₂, C₃, and C₄) through two different routes. The first set
 483 of reactions (**Eqs. (19-20)**) results in H₂O generation ^{57, 58} whereas the second set (**Eqs. (21-**
 484 **22)**) produces CO₂ instead ⁵⁹. The CO₂ by-product method is more feasible than the method
 485 with H₂O formation as shown in **Table 4**.



486
 487 Alkane and alkene products in general are generated primarily through the CO₂ route
 488 particularly in media where CO₂ is highly absorbed (molten carbonates). The absorption of
 489 some amounts of generated CO₂ can be sustained in the molten salt, driving the reactions (**Eqs.**
 490 **(21-22)**) to the right side and increasing hydrocarbon formation. Moreover, due to the primary
 491 production of higher CO rates and in contrast lower H₂ rates, alkene hydrocarbons were found
 492 in a higher proportion than the corresponding alkanes in the final cathodic product. The ΔG
 493 data values (**Table 4**) confirm that the formation of higher hydrocarbon molecules (C₂-C₄) was
 494 possible through the production of CO₂ for alkanes rather than alkenes by the process of Fischer
 495 Tropsch reaction.

496
 497 Therefore, as far as adequate amounts of CO and H₂ gases are produced from electrolysis, there
 498 is sufficient availability for combining on the cathode surface producing alkanes. While the
 499 justification for the formation of alkenes such as C₂H₄, C₃H₆, C₄H₈, rather than alkanes can be

500 provided by the partial oxidation of CH₄ gas. These conditions hold true particularly at a lower
501 CO₂ absorption level due to the feasible partial oxidation of CH₄ to C₂H₄ rather than C₂H₆.



502

503 The oxidation of CH₄ can be performed in two ways. Firstly, CH₄ gas can react directly with
504 O₂ formed at the anode during the co-electrolysis of CO₂ and H₂O (**Eqs. (23-24)**) or also can
505 react with O₂ absorbed inside the molten salt for a short time prior to passing through the anode
506 ceramic tube or being eluted with the cathodic gas product by the draft of feed gas. Secondly,
507 the absorbed O₂ can be transferred to a more reactive oxide anion like peroxide (diatomic O₂²⁻
508 or monoatomic O⁻), playing a significant role in the methane oxidation mechanism particularly
509 in the case of low CO₂ concentration levels. It can also be seen from **Table 4** that the formation
510 of higher molecular weight hydrocarbons (>C₂) will be more feasible (resulting in a more
511 negative ΔG) by this mechanism with the priority on alkenes rather than alkanes.

512

513 The formation of C₂H₆, C₃H₈ and C₄H₁₀ was relatively small compared with the corresponding
514 alkenes as also seen by GC-MS analysis (**Fig. 14**) as the peaks 57, 43 and 29 stands for the
515 mass of fragments lost from C₄H₁₀ (CH₃CH₂CH₂CH₃), C₃H₈ (CH₃CH₂CH₃) and C₂H₆
516 (CH₃CH₃) respectively. The last peaks (43 and 29) are produced from the further fragmentation
517 of C₃H₈ and C₄H₁₀. Peaks 55 and 41 stands for the mass of fragments lost from 1-C₄H₈ (for
518 instance) and C₃H₆ respectively. Peak 15 is showing the mass fragment (methyl) lost from
519 C₄H₁₀, C₃H₈ and C₂H₆. Branco *et al.*^{60, 61} also stated the higher hydrocarbon production (C₂-
520 C₄) through partial oxidation of methane in molten salt electrolytes.

521 **Energy consumption and heating values**

522 The energy required for the conversion of CO₂ to carbon/hydrocarbons will be that needed to
523 carry out the electrolysis and heating up of the molten salt ⁴⁵. If the heating values or energy
524 supplied from the produced fuels are able to compensate some or all the energy consumed
525 while performing electrolysis, the process feasibility increases⁶². This is because the yield of
526 heat generated from the produced hydrocarbon fuel can compensate or substitute some of the
527 normal electricity employed in large scale industrial applications. In the case of molten chloride
528 (KCl-LiCl; 41–59 mol%) electrolyte, the heating value obtained is 162 J from the produced
529 fuel (H₂ and CH₄) with the energy consumption of 278 J. While the heating values obtained
530 are 136 and 170 J from the produced fuels (H₂ and CH₄) by using KOH-NaOH (50: 50 mol%)
531 and LiOH-NaOH (27:73 mol%) respectively. And with the energy consumption of 1200 and
532 1000 J in KOH-NaOH (50: 50 mol%) and LiOH-NaOH (27:73 mol%) electrolysis respectively
533 (see **Table 2**).

534

535 The greater the production of higher hydrocarbons (C₁-C₄), the greater the faraday efficiency
536 and subsequent energy profit attained due to their ability to produce more heating energy
537 (**Table 3**). It is very interesting to note that the energy obtained from the summation of heating
538 values of cathodic products in Li₂CO₃-Na₂CO₃-K₂CO₃ (43.5 : 31.5 : 25 mol%) case was 94.6 J
539 while the total consumed energy was 114.2 J with about 100% of faraday efficiency (**Table 3**).

540 The higher total efficiency results in significantly lower energy consumption of 114 J for the
541 total fuel produced or just 0.157 kWh per mole of fuel. This value is apparently less than the
542 energy consumed for an optimum deposit carbon operation of 0.456 kWh per mole of carbon
543 ⁵⁶. As in all the cases, the produced hydrocarbon fuels are able to provide sufficient heating
544 values so the CO₂-H₂O co-electrolysis processes are considered successful. Tang *et al.* ⁵⁴ has

545 optimized energy consumption for producing 1 kg of carbon from CO₂ as low as 35.59 kW h
546 with a current efficiency of 87.86% under a constant cell voltage of 3.5 V in molten carbonates.

547 **Conclusions**

548 This study presents a new method of CO₂-H₂O conversion into hydrocarbon fuel via molten
549 salts electrolysis at relatively low temperature that is a dire need of hydrocarbon production.
550 The synthesis method generated methane and hydrogen gases by a direct simultaneous splitting
551 of CO₂ and H₂O in LiCl-KCl (58.5: 41.5 mol%), LiOH-NaOH (27: 73 mol%), KOH-NaOH
552 (50: 50 mol%) and Li₂CO₃-Na₂CO₃-K₂CO₃ (43.5 : 31.5 : 25 mol%) electrolyte mixtures. The
553 optimization of each electrolyte was done in the gas feed introduction method (GFOE and
554 GFIE) for obtaining more fuel production. In the case of KCl-LiCl (41: 59 mol%), CH₄ (0.67
555 μmol/h.cm²) and H₂ (32 μmol/h.cm²) were produced with GFIE mode at atmospheric pressure.
556 While in molten hydroxide (LiOH-NaOH; 27: 73 mol %), the H₂ was the predominant gas due
557 to H₂O electrolysis which contributed majorly to the production of CH₄ by reacting with CO₂.
558 The hydrocarbon production rate increased (CH₄: 1.02 to 6.12 μmol h/cm²) by changing the
559 feed gas insertion mode from GFOE to GFIE by using a ceramic tube. In case of molten
560 carbonate, the production rate of CO (11.70 μmol/h.cm²) was significantly higher than H₂ (4.40
561 μmol/h.cm²) in cathodic gas product. Along with H₂ and CO, other hydrocarbon species such
562 as CH₄ and olefins were also produced in molten carbonate case with 99 % of faraday efficiency
563 while other being 59.30% and 87.70% in molten chloride and molten hydroxides respectively.
564 Moreover, the suitable conditions at which the fuel production was achievable are 375 °C, 275
565 °C and 475 °C for molten chlorides, molten hydroxides and molten carbonates under the cell
566 voltage of 2V, 2V and 1.5 V respectively. The proposed technique holds promise as a method
567 for converting electrical energy produced from renewable power sources into conventional
568 fuel, this should be used in future with increased production concentrations.

569 **Supporting information**

570 Phase diagram in mole percentages for binary mixtures of (a) chloride (LiCl-KCl) (b)
571 hydroxide (LiOH-NaOH) and (c) hydroxide (KOH-NaOH) salts (**Fig. S1**) and phase diagram
572 of Li_2CO_3 - Na_2CO_3 - K_2CO_3 ternary molten salt (**Fig. S2**).

573 **Acknowledgement**

574 The authors are grateful for the financial supports from the EPSRC (EP/J000582/1 and
575 EP/F026412/1) and Ningbo Municipal People's Governments (3315 Plan and 2014A35001-1).

576 **References**

- 577 1. Lei, L.; Liu, T.; Fang, S.; Lemmon, J. P.; Chen, F., The co-electrolysis of CO₂-H₂
578 O to methane via a novel micro-tubular electrochemical reactor. *J. Mater. Chem. A* 2017, 5 (6),
579 2904-2910, DOI 10.1039/C6TA10252B.
- 580 2. Ren, J.; Yu, A.; Peng, P.; Lefler, M.; Li, F.-F.; Licht, S., Recent Advances in Solar
581 Thermal Electrochemical Process (STEP) for Carbon Neutral Products and High Value
582 Nanocarbons. *Acc. Chem. Res.* 2019, 52 (11), 3177-3187, DOI 10.1021/acs.accounts.9b00405.
- 583 3. Christensen, E.; Petrushina, I.; Nikiforov, A. V.; Berg, R. W.; Bjerrum, N. J.,
584 CsH₂PO₄ as Electrolyte for the Formation of CH₄ by Electrochemical Eeduction of CO₂. *J.*
585 *Electrochem. Soc.* 2020, 167 (4), 044511, DOI 10.1149/1945-7111/ab75fa.
- 586 4. Skafte, T. L.; Blennow, P.; Hjelm, J.; Graves, C., Carbon deposition and sulfur
587 poisoning during CO₂ electrolysis in nickel-based solid oxide cell electrodes. *J. Power Sources*
588 2018, 373, 54-60, DOI 10.1016/j.jpowsour.2017.10.097.
- 589 5. Sher, F.; Iqbal, S. Z.; Liu, H.; Imran, M.; Snape, C. E., Thermal and kinetic analysis
590 of diverse biomass fuels under different reaction environment: A way forward to renewable
591 energy sources. *Energy Convers. Manage.* 2020, 203, 112266, DOI
592 10.1016/j.enconman.2019.112266.
- 593 6. Abu Hassan, M. H.; Sher, F.; Zarren, G.; Suleiman, N.; Tahir, A. A.; Snape, C. E.,
594 Kinetic and thermodynamic evaluation of effective combined promoters for CO₂ hydrate
595 formation. *J. Nat. Gas Sci. Eng.* 2020, 78, 103313, DOI 10.1016/j.jngse.2020.103313.
- 596 7. Kumaravel, V.; Bartlett, J.; Pillai, S. C., Photoelectrochemical conversion of carbon
597 dioxide (CO₂) into fuels and value-added products. *ACS Energy Lett.* 2020, DOI
598 10.1021/acsenerylett.9b02585.
- 599 8. Anwar, M.; Fayyaz, A.; Sohail, N.; Khokhar, M.; Baqar, M.; Yasar, A.; Rasool, K.;
600 Nazir, A.; Raja, M.; Rehan, M., CO₂ utilization: Turning greenhouse gas into fuels and
601 valuable products. *J. Environ. Manage.* 2020, 260, 110059, DOI
602 10.1016/j.jenvman.2019.110059.
- 603 9. Sastre, F.; Muñoz-Batista, M. J.; Kubacka, A.; Fernández-García, M.; Smith, W. A.;
604 Kapteijn, F.; Makkee, M.; Gascon, J., Efficient Electrochemical Production of Syngas from
605 CO₂ and H₂O by using a Nanostructured Ag/g-C₃N₄ Catalyst. *ChemElectroChem* 2016, 3 (9),
606 1497-1502, DOI 10.1002/celec.201600392.
- 607 10. Wu, H.; Ji, D.; Li, L.; Yuan, D.; Zhu, Y.; Wang, B.; Zhang, Z.; Licht, S., A new
608 technology for efficient, high yield carbon dioxide and water transformation to methane by
609 electrolysis in molten salts. *Adv. Mater. Technol.* 2016, 1 (6), 1600092, DOI
610 10.1002/admt.201600092.
- 611 11. Li, Z.; Zhang, W.; Ji, D.; Liu, S.; Cheng, Y.; Han, J.; Wu, H., Electrochemical
612 Conversion of CO₂ into Valuable Carbon Nanotubes: The Insights into Metallic Electrodes
613 Screening. *J. Electrochem. Soc.* 2020, 167 (4), 042501, DOI 10.1149/1945-7111/ab7176.
- 614 12. Long, C.; Li, X.; Guo, J.; Shi, Y.; Liu, S.; Tang, Z., Electrochemical reduction of
615 CO₂ over heterogeneous catalysts in aqueous solution: recent progress and perspectives. *Small*
616 *Methods* 2019, 3 (3), 1800369, DOI 10.1002/smt.201800369.
- 617 13. Moura de Salles Pupo, M.; Kortlever, R., Electrolyte effects on the electrochemical
618 reduction of CO₂. *ChemPhysChem* 2019, 20 (22), 2926-2935, DOI 10.1002/cphc.201900680.
- 619 14. Chen, Y.; Wang, M.; Lu, S.; Tu, J.; Jiao, S., Electrochemical graphitization conversion
620 of CO₂ through soluble NaVO₃ homogeneous catalyst in carbonate molten salt. *Electrochim.*
621 *Acta* 2020, 331, 135461, DOI 10.1016/j.electacta.2019.135461.
- 622 15. Kusama, S.; Saito, T.; Hashiba, H.; Sakai, A.; Yotsuhashi, S., Crystalline copper (II)
623 phthalocyanine catalysts for electrochemical reduction of carbon dioxide in aqueous media.
624 *ACS Catal.* 2017, 7 (12), 8382-8385, DOI 10.1021/acscatal.7b02220.

- 625 16. Acar, C.; Dincer, I., Review and evaluation of hydrogen production options for better
626 environment. *J. Cleaner Prod.* 2019, 218, 835-849, DOI 10.1016/j.jclepro.2019.02.046.
- 627 17. Al-Shara, N. K.; Sher, F.; Iqbal, S. Z.; Curnick, O.; Chen, G. Z., Design and
628 optimization of electrochemical cell potential for hydrogen gas production. *J. Energy Chem.*
629 2021, 52, 421-427, DOI 10.1016/j.jechem.2020.04.026.
- 630 18. Luo, Y.; Shi, Y.; Chen, Y.; Li, W.; Jiang, L.; Cai, N., Pressurized Tubular Solid
631 Oxide H₂O/CO₂ Co-electrolysis Cell for Direct Power-to-Methane. *AIChE J.* 2020, e16896,
632 DOI 10.1002/aic.16896.
- 633 19. Kamali, A. R., Production of Advanced Materials in Molten Salts. In *Green Production*
634 *of Carbon Nanomaterials in Molten Salts and Applications*, Springer: 2020; pp 5-18, DOI
635 10.1007/978-981-15-2373-1_2.
- 636 20. Dogu, D.; Gunduz, S.; Meyer, K. E.; Deka, D. J.; Ozkan, U. S., CO₂ and H₂O
637 Electrolysis Using Solid Oxide Electrolyzer Cell (SOEC) with La and Cl-doped Strontium
638 Titanate Cathode. *Catal. Lett.* 2019, 149 (7), 1743-1752, DOI 10.1007/s10562-019-02786-8.
- 639 21. Wu, H.; Liu, Y.; Ji, D.; Li, Z.; Yi, G.; Yuan, D.; Wang, B.; Zhang, Z.; Wang, P.,
640 Renewable and high efficient syngas production from carbon dioxide and water through solar
641 energy assisted electrolysis in eutectic molten salts. *J. Power Sources* 2017, 362, 92-104, DOI
642 10.1016/j.jpowsour.2017.07.016.
- 643 22. Xu, H.; Chen, B.; Irvine, J.; Ni, M., Modeling of CH₄-assisted SOEC for H₂O/CO₂
644 co-electrolysis. *Int. J. Hydrogen Energy* 2016, 41 (47), 21839-21849, DOI
645 10.1016/j.ijhydene.2016.10.026.
- 646 23. Tang, D.; Dou, Y.; Yin, H.; Mao, X.; Xiao, W.; Wang, D., The capacitive
647 performances of carbon obtained from the electrolysis of CO₂ in molten carbonates: Effects of
648 electrolysis voltage and temperature. *J. Energy Chem.* 2019, DOI
649 10.1016/j.jechem.2019.11.006.
- 650 24. Ji, D.; Li, Z.; Li, W.; Yuan, D.; Wang, Y.; Yu, Y.; Wu, H., The optimization of
651 electrolyte composition for CH₄ and H₂ generation via CO₂/H₂O co-electrolysis in eutectic
652 molten salts. *Int. J. Hydrogen Energy* 2019, 44 (11), 5082-5089, DOI
653 10.1016/j.ijhydene.2018.09.089.
- 654 25. Liu, Y.; Ji, D.; Li, Z.; Yuan, D.; Jiang, M.; Yang, G.; Yu, Y.; Wang, Y.; Wu, H.,
655 Effect of CaCO₃ addition on the electrochemical generation of syngas from CO₂/H₂O in
656 molten salts. *Int. J. Hydrogen Energy* 2017, 42 (29), 18165-18173, DOI
657 10.1016/j.ijhydene.2017.04.160.
- 658 26. Xiao, W.; Wang, D.-H., Rare metals preparation by electro-reduction of solid
659 compounds in high-temperature molten salts. *Rare Met.* 2016, 35 (8), 581-590, DOI
660 10.1007/s12598-016-0778-4.
- 661 27. Ijje, H. V.; Sun, C.; Chen, G. Z., Indirect electrochemical reduction of carbon dioxide
662 to carbon nanopowders in molten alkali carbonates: Process variables and product properties.
663 *Carbon* 2014, 73, 163-174, DOI 10.1016/j.carbon.2014.02.052.
- 664 28. Liu, Y.; Yuan, D.; Ji, D.; Li, Z.; Zhang, Z.; Wang, B.; Wu, H., Syngas production:
665 diverse H₂/CO range by regulating carbonates electrolyte composition from CO₂/H₂O via
666 co-electrolysis in eutectic molten salts. *RSC Adv.* 2017, 7 (83), 52414-52422, DOI
667 10.1039/C7RA07320H.
- 668 29. Weng, W.; Tang, L.; Xiao, W., Capture and electro-splitting of CO₂ in molten salts. *J.*
669 *Energy Chem.* 2019, 28, 128-143, DOI 10.1016/j.jechem.2018.06.012.
- 670 30. Ge, J.; Hu, L.; Wang, W.; Jiao, H.; Jiao, S., Electrochemical Conversion of CO₂ into
671 Negative Electrode Materials for Li-Ion Batteries. *ChemElectroChem* 2015, 2 (2), 224-230,
672 DOI 10.1002/celec.201402297.
- 673 31. Deng, B.; Chen, Z.; Gao, M.; Song, Y.; Zheng, K.; Tang, J.; Xiao, W.; Mao, X.;
674 Wang, D., Molten salt CO₂ capture and electro-transformation (MSCC-ET) into capacitive

675 carbon at medium temperature: effect of the electrolyte composition. *Faraday Discuss.* 2016,
676 190, 241-258, DOI 10.1039/C5FD00234F.

677 32. Ren, J.; Johnson, M.; Singhal, R.; Licht, S., Transformation of the greenhouse gas
678 CO₂ by molten electrolysis into a wide controlled selection of carbon nanotubes. *J. CO₂ Util.*
679 2017, 18, 335-344, DOI 10.1016/j.jcou.2017.02.005.

680 33. Douglas, A.; Carter, R.; Muralidharan, N.; Oakes, L.; Pint, C. L., Iron catalyzed
681 growth of crystalline multi-walled carbon nanotubes from ambient carbon dioxide mediated by
682 molten carbonates. *Carbon* 2017, 116, 572-578, DOI 10.1016/j.carbon.2017.02.032.

683 34. Arcaro, S.; Berutti, F.; Alves, A.; Bergmann, C., MWCNTs produced by electrolysis
684 of molten carbonate: Characteristics of the cathodic products grown on galvanized steel and
685 nickel chrome electrodes. *Appl. Surf. Sci.* 2019, 466, 367-374, DOI
686 10.1016/j.apsusc.2018.10.055.

687 35. Ji, D.; Liu, Y.; Li, Z.; Yuan, D.; Yang, G.; Jiang, M.; Wang, Y.; Yu, Y.; Wu, H., A
688 comparative study of electrodes in the direct synthesis of CH₄ from CO₂ and H₂O in molten
689 salts. *Int. J. Hydrogen Energy* 2017, 42 (29), 18156-18164, DOI
690 10.1016/j.ijhydene.2017.04.152.

691 36. Li, L.; Shi, Z.; Gao, B.; Hu, X.; Wang, Z., Electrochemical conversion of CO₂ to
692 carbon and oxygen in LiCl–Li₂O melts. *Electrochim. Acta* 2016, 190, 655-658, DOI
693 10.1016/j.electacta.2015.12.202.

694 37. Kaplan, V.; Wachtel, E.; Gartsman, K.; Feldman, Y.; Lubomirsky, I., Conversion of
695 CO₂ to CO by electrolysis of molten lithium carbonate. *J. Electrochem. Soc.* 2010, 157 (4),
696 B552-B556, DOI 10.1149/1.3308596.

697 38. Ijije, H. V. Electrochemical conversion of carbon dioxide to carbon in molten carbonate
698 salts. University of Nottingham, Cenrtal Store, 2015.

699 39. Hu, L.; Song, Y.; Ge, J.; Zhu, J.; Han, Z.; Jiao, S., Electrochemical deposition of
700 carbon nanotubes from CO₂ in CaCl₂–NaCl-based melts. *J. Mater. Chem. A* 2017, 5 (13),
701 6219-6225, DOI 10.1039/C7TA00258K.

702 40. Lorenz, P. K.; Janz, G. J., Electrolysis of molten carbonates: anodic and cathodic gas-
703 evolving reactions. *Electrochim. Acta* 1970, 15 (6), 1025-1035, DOI 10.1016/0013-
704 4686(70)80042-1.

705 41. Halmann, M.; Zuckerman, K., Electroreduction of carbon dioxide to carbon monoxide
706 in molten LiCl + KCl, LiF + KF + NaF, Li₂CO₃ + Na₂CO₃ + K₂CO₃ and AlCl₃ + NaCl. *J.*
707 *Electroanal. Chem. Interfacial Electrochem.* 1987, 235 (1), 369-380, DOI 10.1016/0022-
708 0728(87)85221-X.

709 42. Al-Shara, N. K.; Sher, F.; Yaqoob, A.; Chen, G. Z., Electrochemical investigation of
710 novel reference electrode Ni/Ni(OH)₂ in comparison with silver and platinum inert quasi-
711 reference electrodes for electrolysis in eutectic molten hydroxide. *Int. J. Hydrogen Energy*
712 2019, 44 (50), 27224-27236, DOI 10.1016/j.ijhydene.2019.08.248.

713 43. Song, Q.; Xu, Q.; Wang, Y.; Shang, X.; Li, Z., Electrochemical deposition of carbon
714 films on titanium in molten LiCl–KCl–K₂CO₃. *Thin Solid Films* 2012, 520 (23), 6856-6863,
715 DOI 10.1016/j.tsf.2012.07.056.

716 44. Deng, B.; Tang, J.; Gao, M.; Mao, X.; Zhu, H.; Xiao, W.; Wang, D., Electrolytic
717 synthesis of carbon from the captured CO₂ in molten LiCl–KCl–CaCO₃: Critical roles of
718 electrode potential and temperature for hollow structure and lithium storage performance.
719 *Electrochim. Acta* 2018, 259, 975-985 DOI 10.1016/j.electacta.2017.11.025.

720 45. Ijije, H. V.; Lawrence, R. C.; Chen, G. Z., Carbon electrodeposition in molten salts:
721 electrode reactions and applications. *RSC Adv.* 2014, 4 (67), 35808-35817, DOI
722 10.1039/C4RA04629C.

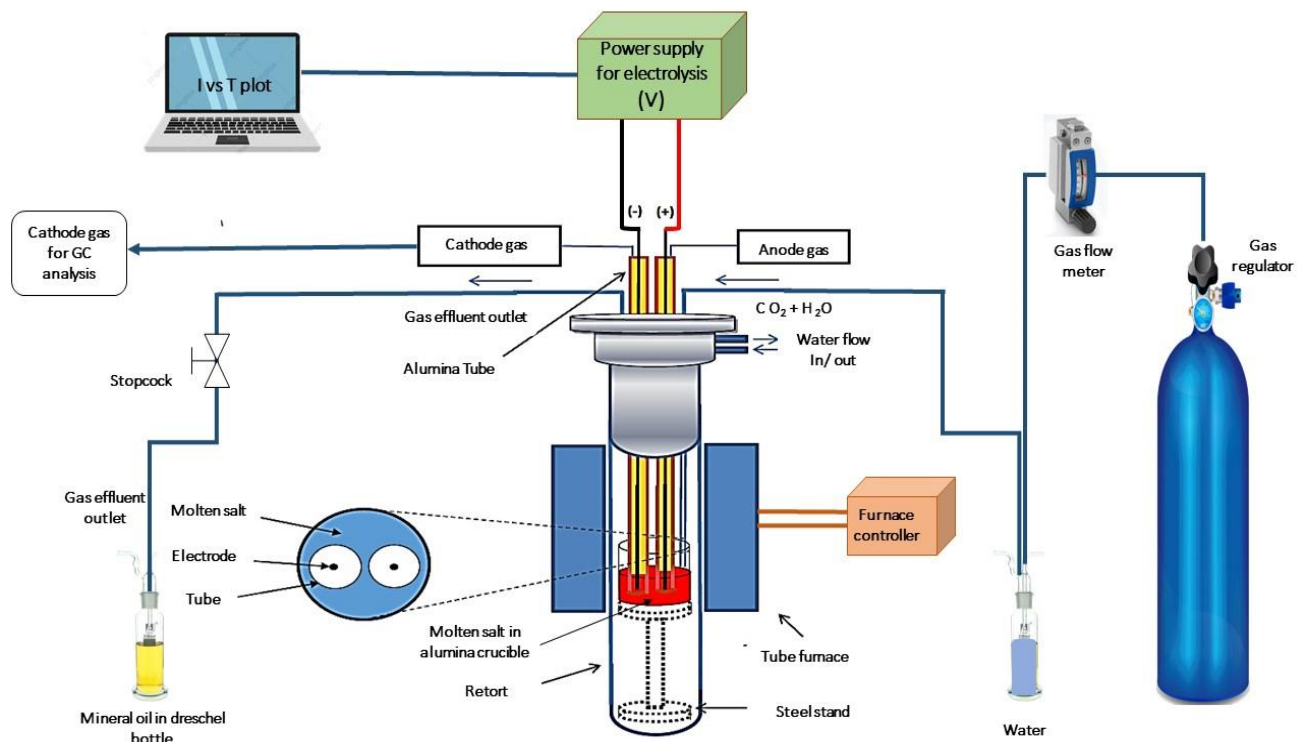
- 723 46. Kamali, A. R.; Fray, D. J., Large-scale preparation of graphene by high temperature
724 insertion of hydrogen into graphite. *Nanoscale* 2015, 7 (26), 11310-11320, DOI
725 10.1039/C5NR01132A
- 726 47. Ijije, H. V.; Lawrence, R. C.; Siambun, N. J.; Jeong, S. M.; Jewell, D. A.; Hu, D.;
727 Chen, G. Z., Electro-deposition and re-oxidation of carbon in carbonate-containing molten
728 salts. *Faraday Discuss.* 2014, 172, 105-116, DOI 10.1039/C4FD00046C.
- 729 48. Otake, K.; Kinoshita, H.; Kikuchi, T.; Suzuki, R. O., CO₂ gas decomposition to carbon
730 by electro-reduction in molten salts. *Electrochim. Acta* 2013, 100, 293-299, DOI
731 10.1016/j.electacta.2013.02.076.
- 732 49. Al-Shara, N. K.; Sher, F.; Iqbal, S. Z.; Sajid, Z.; Chen, G. Z., Electrochemical study
733 of different membrane materials for the fabrication of stable, reproducible and reusable
734 reference electrode. *J. Energy Chem.* 2020, 49, 33-41, DOI 10.1016/j.jechem.2020.01.008.
- 735 50. Graves, C.; Ebbesen, S. D.; Mogensen, M.; Lackner, K. S., Sustainable hydrocarbon
736 fuels by recycling CO₂ and H₂O with renewable or nuclear energy. *Renewable Sustainable*
737 *Energy Rev.* 2011, 15 (1), 1-23, DOI 10.1016/j.rser.2010.07.014.
- 738 51. Pardo, P.; Deydier, A.; Anxionnaz-Minvielle, Z.; Rougé, S.; Cabassud, M.; Cognet,
739 P., A review on high temperature thermochemical heat energy storage. *Renewable Sustainable*
740 *Energy Rev.* 2014, 32, 591-610, DOI 10.1016/j.rser.2013.12.014.
- 741 52. Groult, H.; Le Van, K.; Lantelme, F., Electrodeposition of carbon-metal powders in
742 alkali carbonate melts. *J. Electrochem. Soc.* 2014, 161 (7), D3130-3138, DOI
743 10.1149/2.019407jes.
- 744 53. Chery, D.; Albin, V.; Meléndez-Ceballos, A.; Lair, V.; Cassir, M., Mechanistic
745 approach of the electrochemical reduction of CO₂ into CO at a gold electrode in molten
746 carbonates by cyclic voltammetry. *Int. J. Hydrogen Energy* 2016, 41 (41), 18706-18712 DOI
747 10.1016/j.ijhydene.2016.06.094.
- 748 54. Tang, D.; Yin, H.; Mao, X.; Xiao, W.; Wang, D., Effects of applied voltage and
749 temperature on the electrochemical production of carbon powders from CO₂ in molten salt
750 with an inert anode. *Electrochim. Acta* 2013, 114, 567-573, DOI
751 10.1016/j.electacta.2013.10.109.
- 752 55. Novoselova, I. A.; Kuleshov, S. V.; Volkov, S. V.; Bykov, V. N., Electrochemical
753 synthesis, morphological and structural characteristics of carbon nanomaterials produced in
754 molten salts. *Electrochim. Acta* 2016, 211, 343-355, DOI 10.1016/j.electacta.2016.05.160.
- 755 56. Yin, H.; Mao, X.; Tang, D.; Xiao, W.; Xing, L.; Zhu, H.; Wang, D.; Sadoway, D.
756 R., Capture and electrochemical conversion of CO₂ to value-added carbon and oxygen by
757 molten salt electrolysis. *Energy Environ. Sci.* 2013, 6 (5), 1538-1545, DOI
758 10.1039/C3EE24132G.
- 759 57. Akhmedov, V.; Ismailzadeh, A., The role of CO₂ and H₂O in the formation of gas-
760 oil hydrocarbons: current performance and outlook. *J. Math* 2019, 6 (10).
- 761 58. Torrente-Murciano, L.; Mattia, D.; Jones, M. D.; Plucinski, P. K., Formation of
762 hydrocarbons via CO₂ hydrogenation – A thermodynamic study. *J. CO₂ Util.* 2014, 6, 34-39,
763 DOI 10.1016/j.jcou.2014.03.002.
- 764 59. Jafarbegloo, M.; Tarlani, A.; Mesbah, A. W.; Sahebdehfar, S., Thermodynamic
765 analysis of carbon dioxide reforming of methane and its practical relevance. *Int. J. Hydrogen*
766 *Energy* 2015, 40 (6), 2445-2451, DOI 10.1016/j.ijhydene.2014.12.103.
- 767 60. Branco, J. B.; Lopes, G.; Ferreira, A. C.; Leal, J. P., Catalytic oxidation of methane
768 on KCl-MCl_x (M= Li, Mg, Co, Cu, Zn) eutectic molten salts. *J. Mol. Liq.* 2012, 171, 1-5, DOI
769 10.1016/j.molliq.2012.04.001.
- 770 61. Branco, J. B.; Lopes, G.; Ferreira, A. C., Catalytic oxidation of methane over KCl-
771 LnCl₃ eutectic molten salts. *Catal. Commun.* 2011, 12 (15), 1425-1427, DOI
772 10.1016/j.catcom.2011.05.023.

773 62. Al-Juboori, O.; Sher, F.; Hazafa, A.; Khan, M. K.; Chen, G. Z., The effect of variable
774 operating parameters for hydrocarbon fuel formation from CO₂ by molten salts electrolysis. *J.*
775 *CO₂ Util.* 2020, *40*, 101193, DOI 10.1016/j.jcou.2020.101193.
776

777
778

779
780

List of Figures



781
782
783

Fig. 1. A schematic representation of the experimental setup.

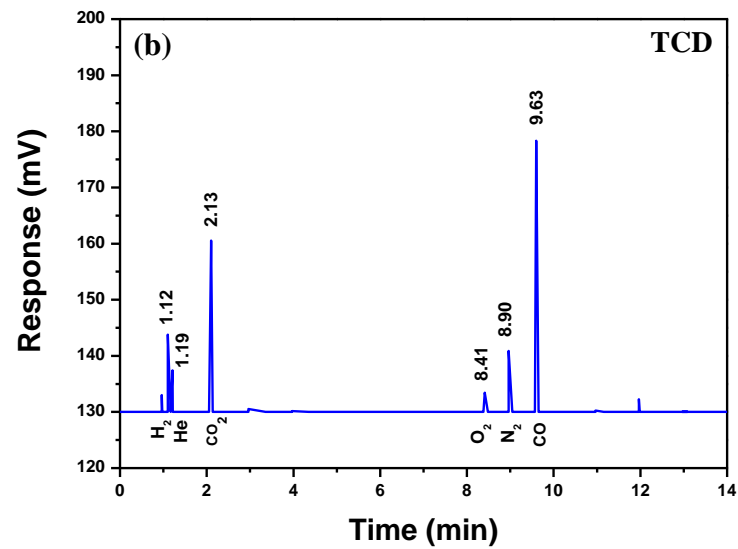
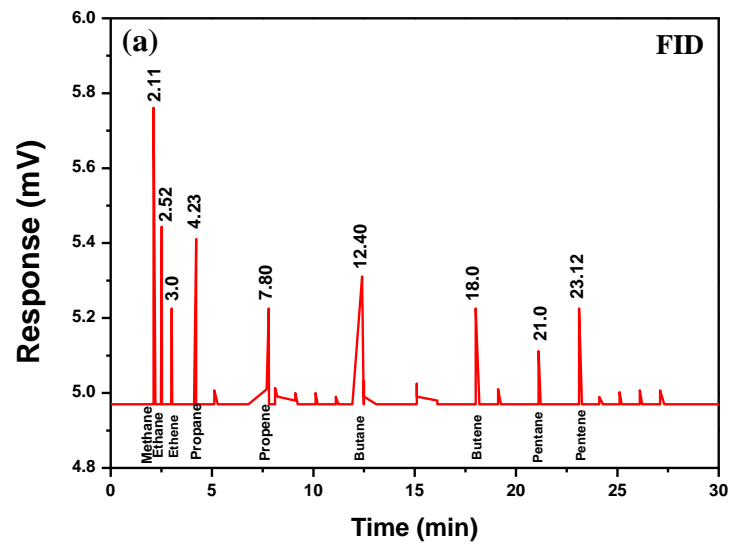


Fig. 2. The gas chromatography analysis of calibration gas standards as reference for the comparison with other electrolysis gaseous products by (a) FID detector (b) TCD detector.

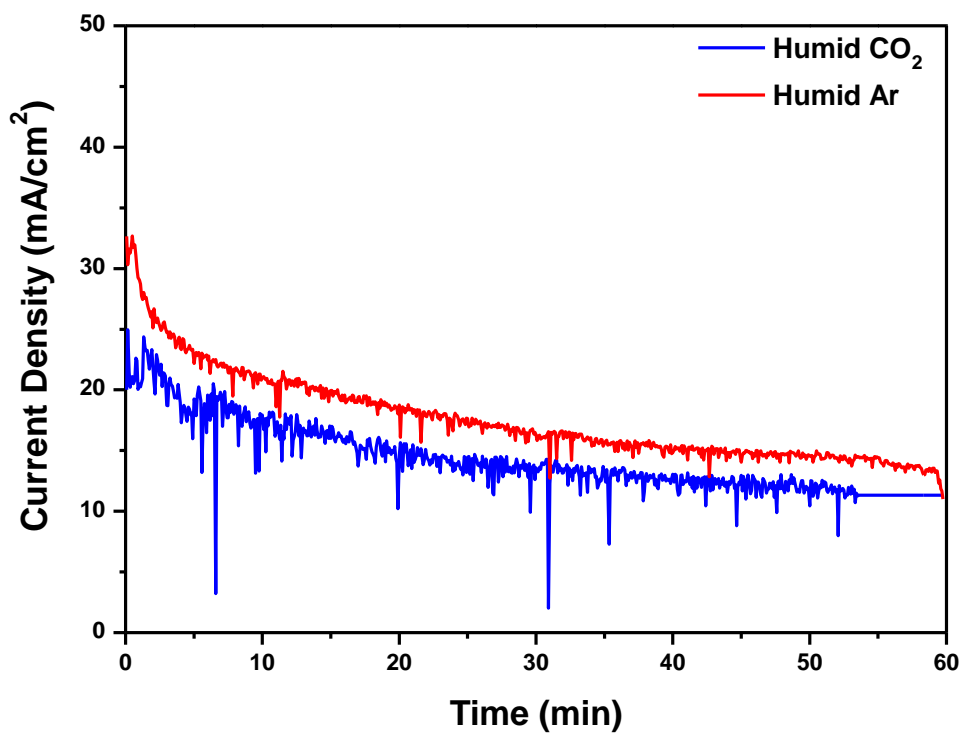


Fig. 3. Current-time curves resulting from electrolysis performed in molten chloride with and without CO₂ at 2V and 375 °C in GFOE mode.

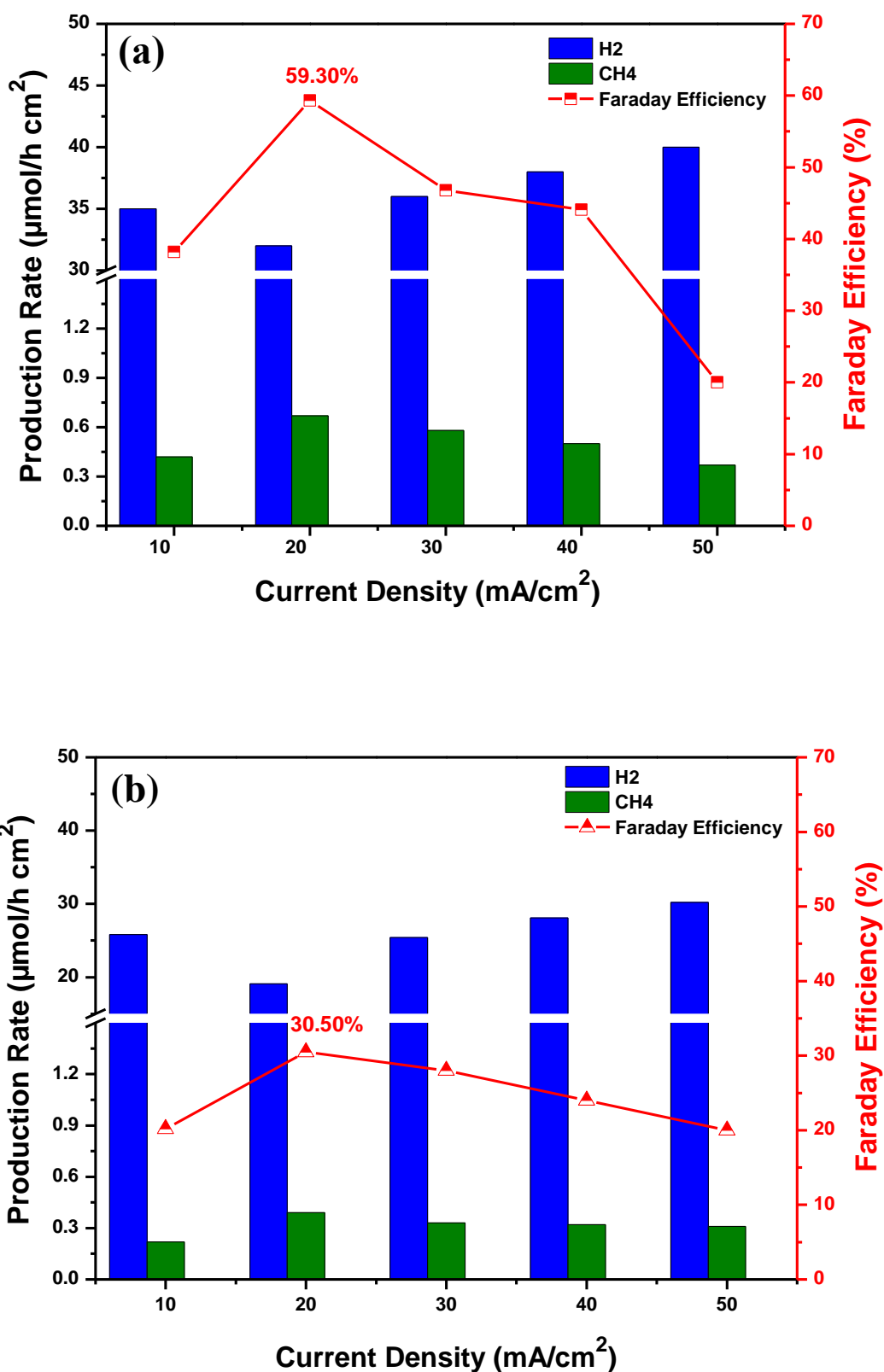


Fig. 4. The faraday efficiency and production rates of gaseous products at 2 V and 375 °C under different current density in case of molten chloride electrolysis during GFIE mode after (a) 30 min (b) 60 min.

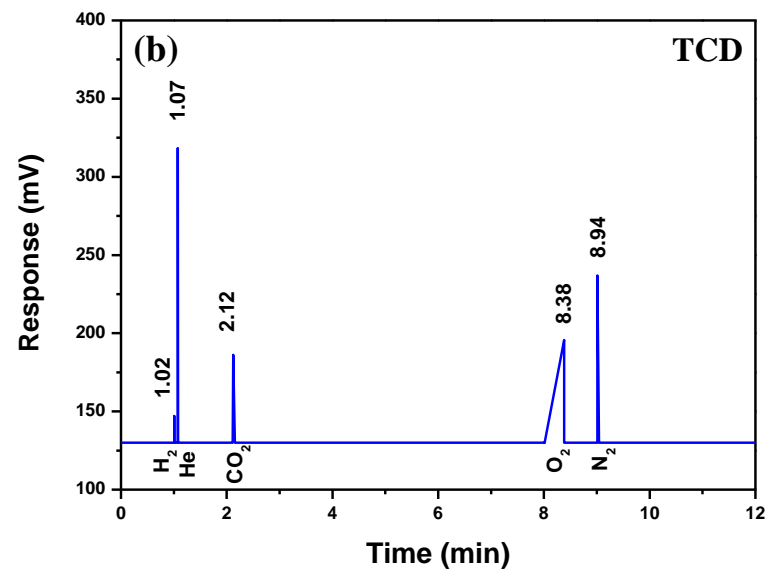
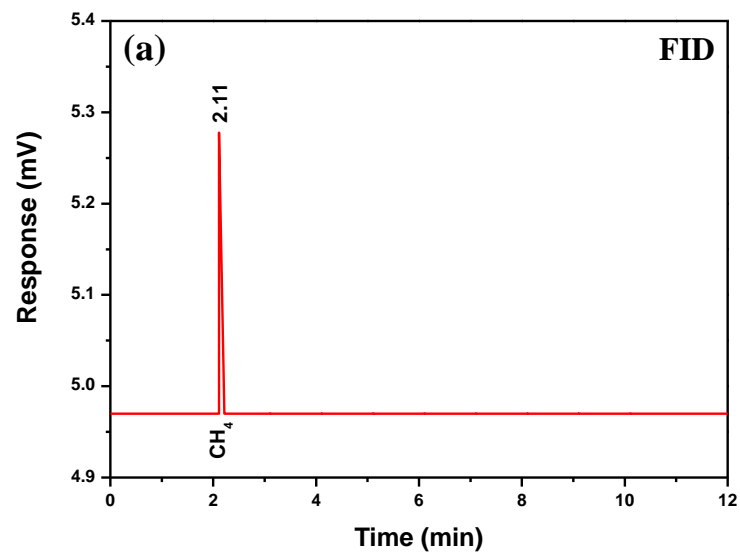


Fig. 5. The gas chromatography analysis of gaseous products in case of molten chloride electrolysis at 375 °C and 2 V by (a) FID detector (b) TCD detector.

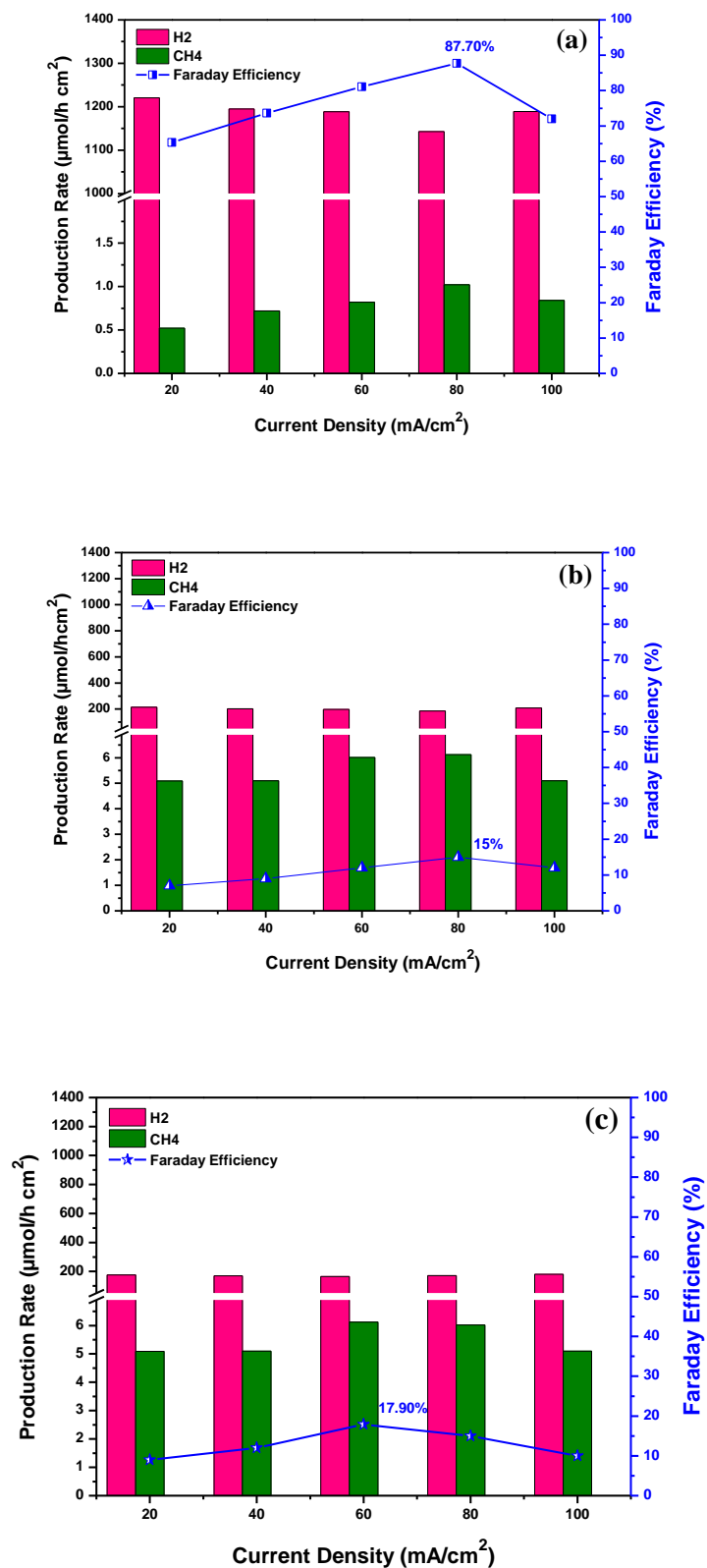


Fig. 6. The faraday efficiency and production rates of gaseous products at 2 V under different current density after electrolysis in; (a) LiOH-NaOH with GFOE mode at 275 °C (b) LiOH-NaOH with GFIE mode at 275 °C (c) KOH-NaOH with GFIE mode at 225 °C.

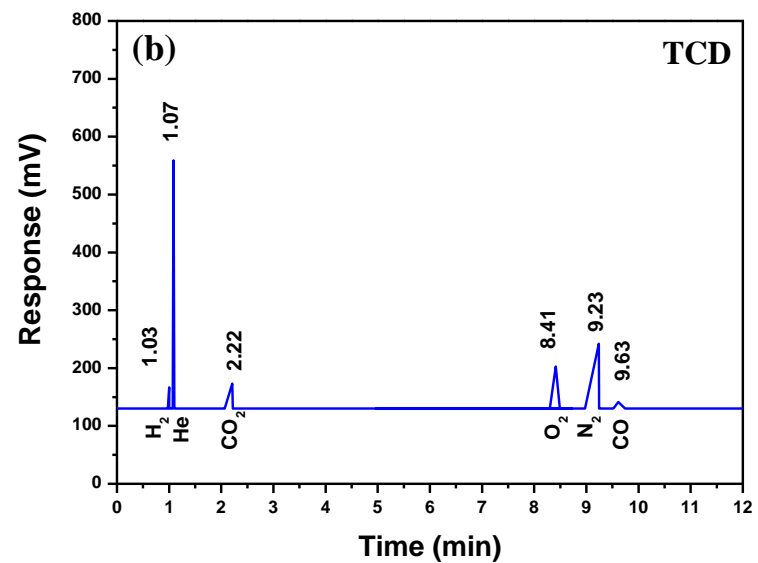
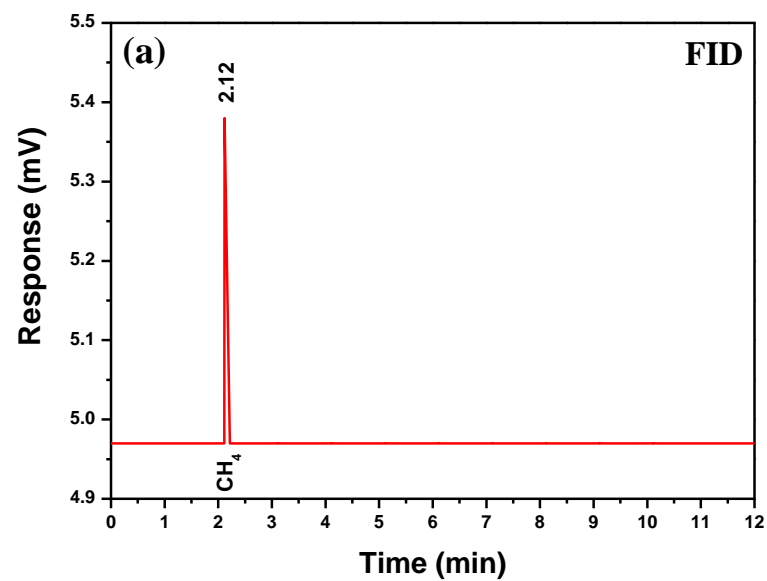


Fig. 7. The gas chromatography analysis of gaseous products in case of molten hydroxide (LiOH-NaOH) electrolysis by (a) FID detector (b) TCD detector.

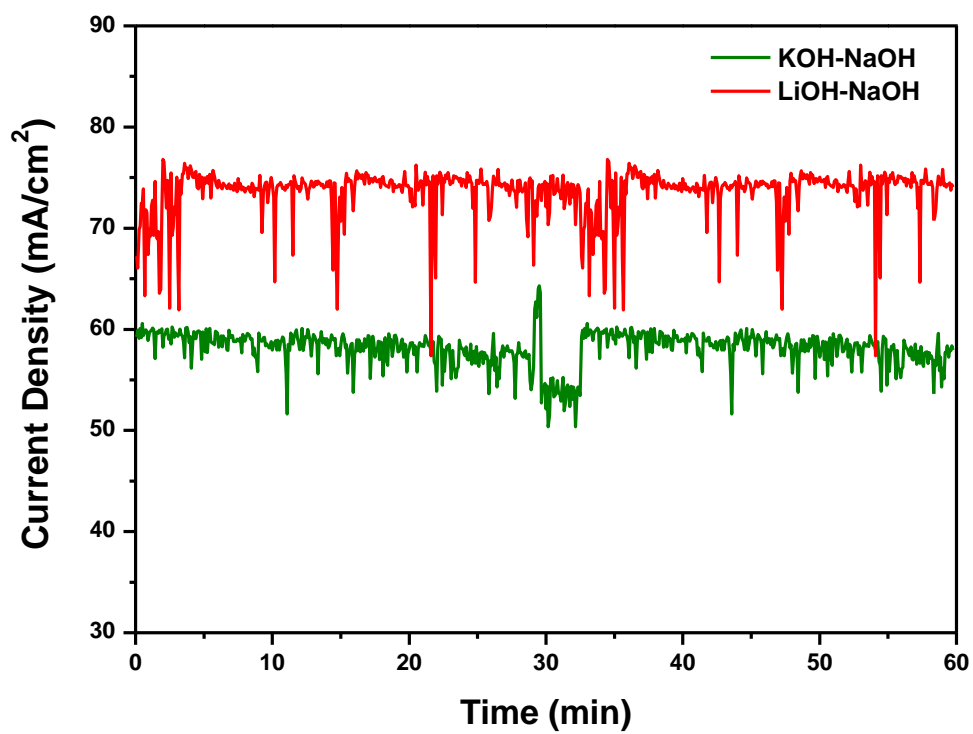


Fig. 8. Current-time curves resulting from electrolysis performed in two different molten hydroxides at 2V.

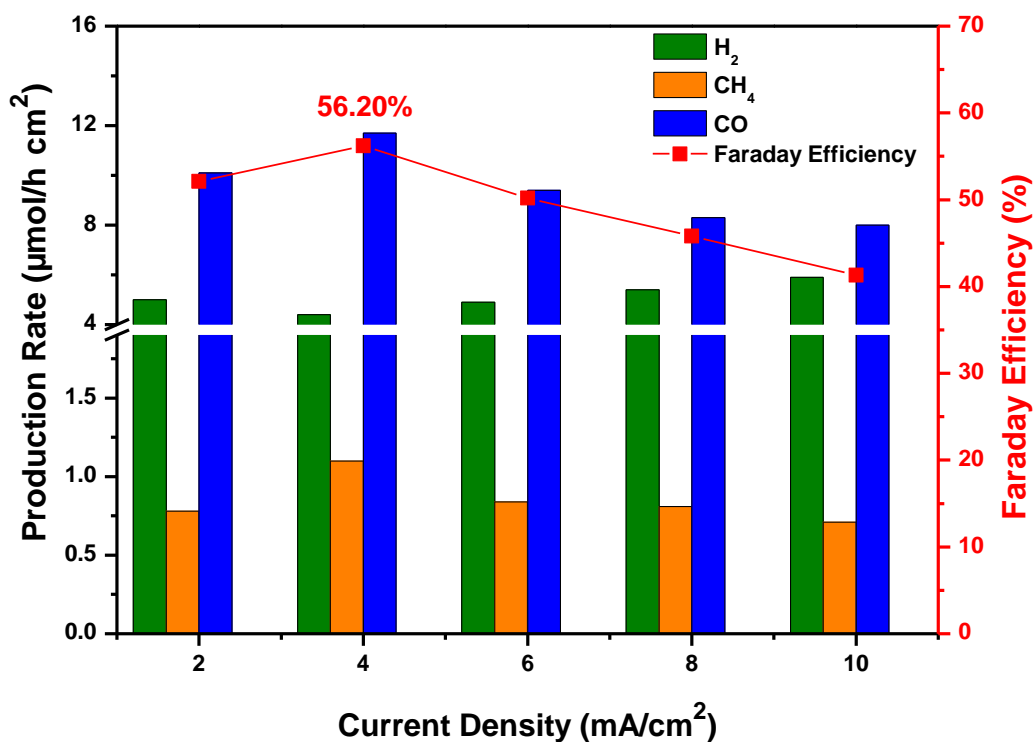


Fig. 9. The faraday efficiency and production rate of gaseous products at 1.5 V and 425 °C under different current density in molten carbonate electrolyte.

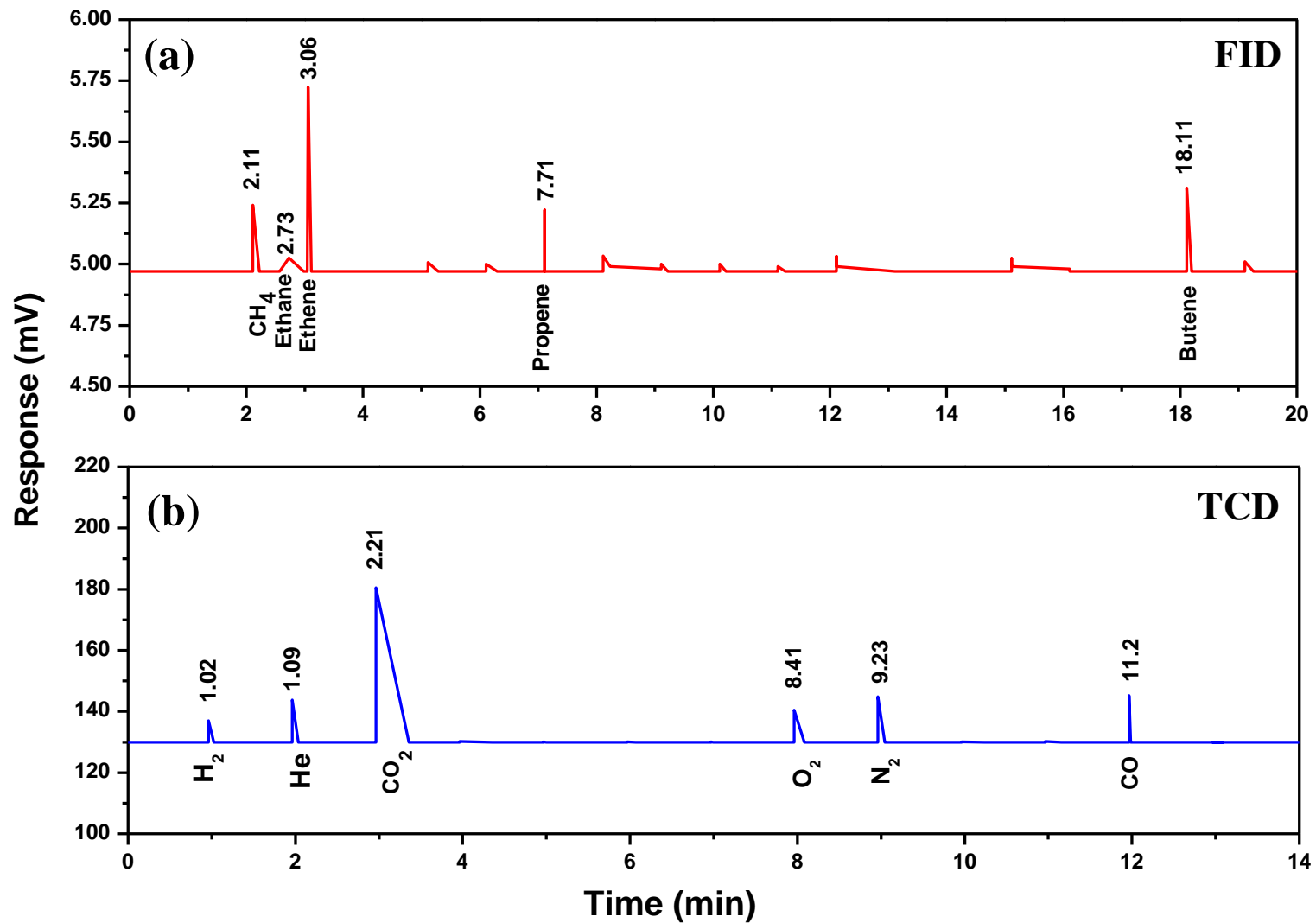


Fig. 10. The gas chromatography analysis of gaseous products in case of molten carbonate electrolysis by (a) FID detector (b) TCD detector.

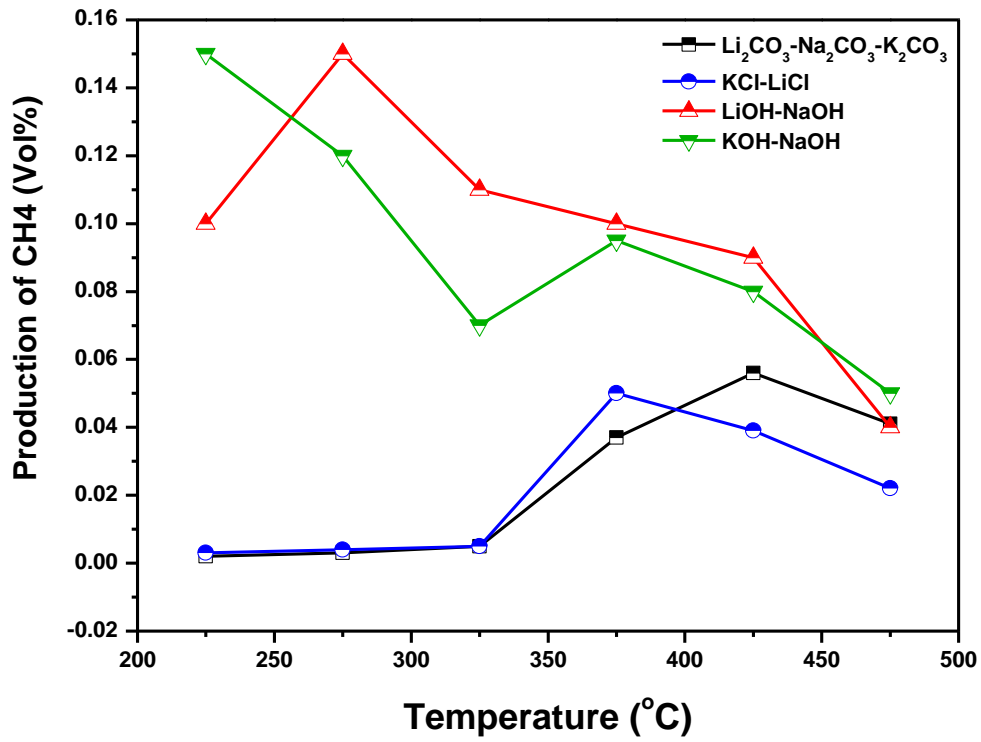


Fig. 11. The selection of optimum temperatures for all electrolytes on the basis of CH_4 production.

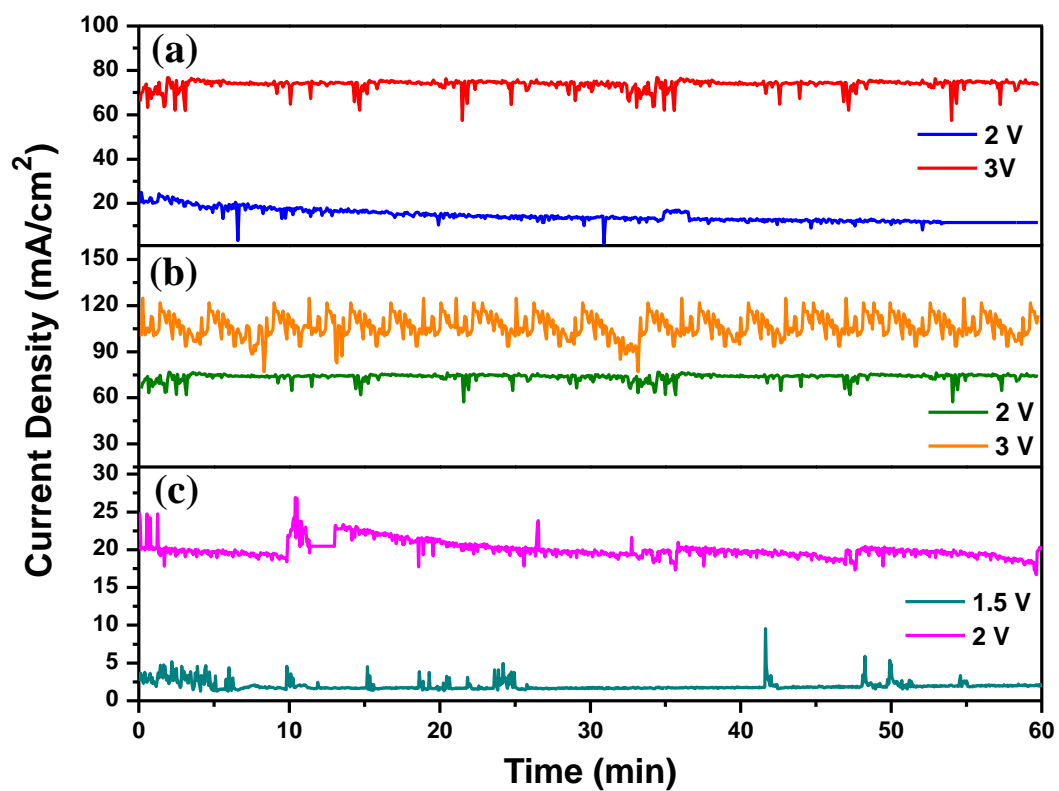


Fig. 12. The current density vs time plot at different voltages for three types of electrolytes; (a) molten chloride, (b) molten hydroxide and (c) molten carbonate.

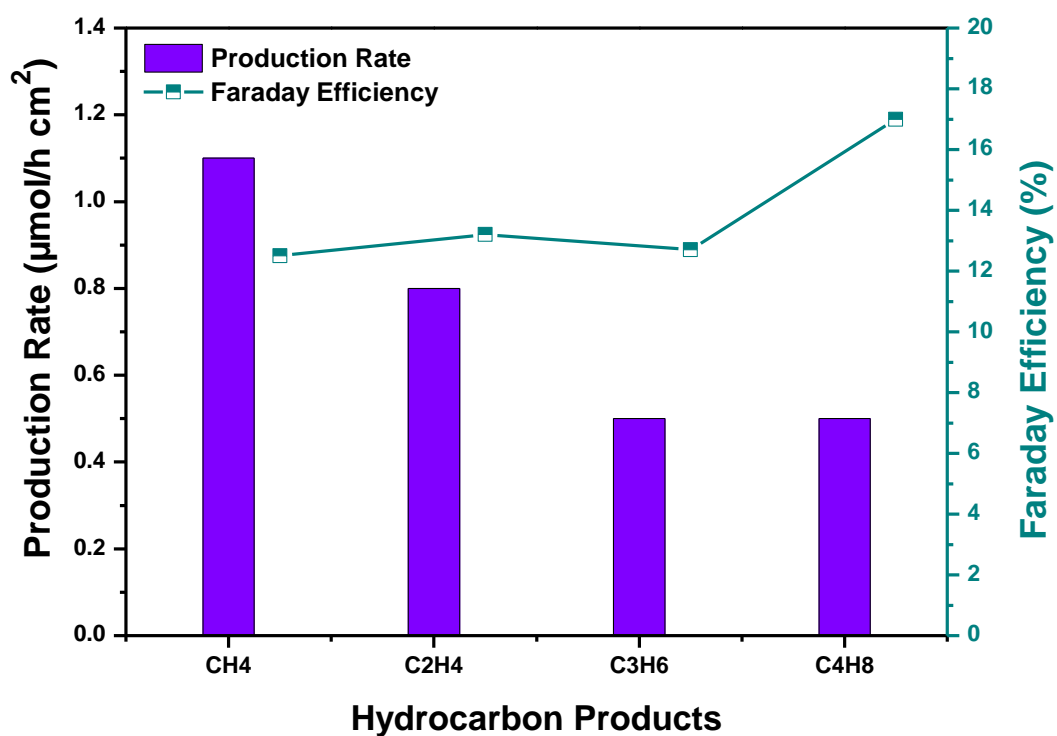


Fig. 13. The faraday efficiency and production rates of higher hydrocarbons at 1.5 V and 425 °C in case of molten carbonate electrolysis.

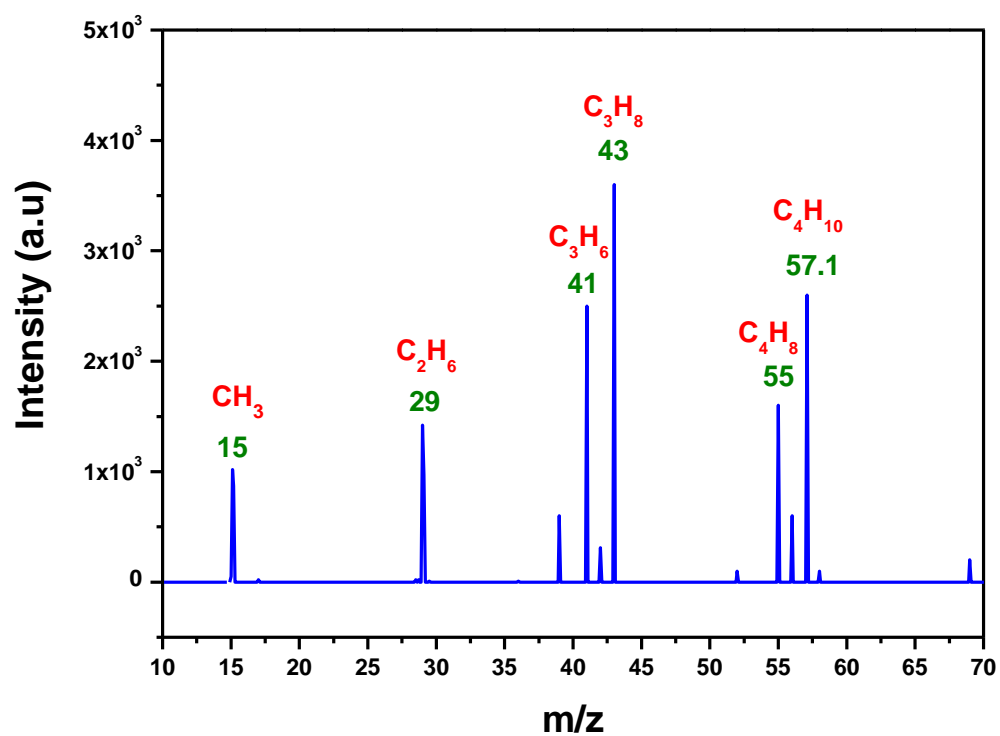


Fig. 14. The mass spectrum of compounds showing hydrocarbon after electrolysis in molten carbonate electrolyte under 1.5 V at 425 °C.

List of Tables

Table 1. Specification of cathodic gas products in molten chloride salt with GFIE mode of electrolysis at 2V and 375 °C by using GC analysis.

Products	Gas product composition (vol. %)		Uncertainty of gas composition		Faraday efficiency (%)		Energy consumption (J)	
	(30 min)	(60 min)	(30 min)	(60 min)	(30 min)	(60 min)	(30 min)	(60 min)
H ₂	2.40	2.48	±0.10	± 0.10	54.80	28.20		
CH ₄	0.05	0.05	±0.005	±0.005	4.50	2.30	278.00	311.00
CO	0.00	0.00	0.00	0.00	0.00	0.00		
CO ₂	34.80	4.84	–	–	–	–		
H ₂ O	2.00	2.00	–	–	–	–		
Ar	60.70	90.60	–	–	–	–		

Table 2. Specification of cathodic gas products during electrolysis in molten hydroxide (LiOH-NaOH) at 275 °C and (KOH-NaOH) at 225 °C under 2V applied voltage using GC analysis.

Products	Gas product composition (vol. %)			Uncertainty of gas composition			Faraday efficiency (%)			Heating values (J)		Energy consumption (J)	
	*LiOH- NaOH	**LiOH- NaOH	**KOH- NaOH	*LiOH- NaOH	**LiOH- NaOH	**KOH -NaOH	*LiOH- NaOH	**LiOH -NaOH	**KOH -NaOH	*LiOH- NaOH	**KOH- NaOH	**LiOH- NaOH	**KOH- NaOH
H ₂	27.3	4.44	3.94	± 0.90	± 0.10	± 0.10	87.30	13.00	15.60	130.00	116.00		
CH ₄	0.03	0.15	0.15	± 0.004	± 0.01	± 0.01	0.40	2.00	2.30	14.00	12.00		
CO	0.00	0.00	0.00	0.00	0.00	0.00	0.00	0.00	0.00	0.00	0.00		
CO ₂	0.480	0.750	0.580	–	–	–	–	–	–	–	–	1200.00	1000.00
H ₂ O	0.00	0.00	0.00	–	–	–	–	–	–	–	–		
Ar	72.20	94.70	95.30	–	–	–	–	–	–	–	–		

* After electrolysis with GFOE mode

** After electrolysis with GFIE mode

Table 3. Specification of cathodic gas products after electrolysis in molten carbonate at 1.5 V and 425 °C by using GC and mass spectrometric analysis.

Product	Gas product composition (vol. %)	Uncertainty of gas composition	Faraday efficiency (%)	Heating value (J)	Energy consumption (J)
H ₂	0.22	±0.04	11.90	11.40	
CH ₄	0.06	±0.005	12.50	10.40	
C ₂ H ₄	0.04	±0.003	13.20	12.00	
C ₃ H ₆	0.03	±0.005	12.70	11.00	114.20
C ₄ H ₈	0.03	±0.002	17.00	14.50	
CO	0.58	±0.09	31.80	35.30	
CO ₂	52.70	–	–	–	
H ₂ O	2.40	–	–	–	
Ar	44.00	–	–	–	

Table 4. List of ΔG and ΔH for the generation of hydrocarbon products from the Fischer-Tropsch reaction (through CO_2 and water formation) and partial oxidation of methane at 425 °C.

Products	Fischer-Tropsch Reaction				CH ₄ partial oxidation	
	ΔG (kJ/mol)		ΔH (kJ/mol)		ΔG (kJ/mol)	ΔH (kJ/mol)
	CO ₂ formed	H ₂ O formed	CO ₂ formed	H ₂ O formed		
CH ₄	-61.41	-48.37	-257.70	-220.10	–	–
C ₂ H ₆	-52.03	-25.94	-445.90	-369.90	-138.20	-175.90
C ₂ H ₄	-2.10	23.98	-303.40	-227.40	-297.20	-278.90
C ₃ H ₈	-39.60	-0.47	-549.30	-435.30	-273.30	-267.10
C ₃ H ₆	-5.69	33.44	-423.70	-309.70	-448.30	-387.00
C ₄ H ₁₀	-43.31	8.86	-722.60	-570.60	-424.50	-428.10
C ₄ H ₈	-18.62	33.55	-710.60	-558.70	-608.80	-661.70

For Table of Contents Use Only

The co-electrolysis of CO₂ and H₂O in molten chloride, molten hydroxides and molten carbonates was performed at moderate temperatures for sustainable hydrocarbons formation.

